LBL-37816
UC-414
Preprint

Lawrence Berkeley Laboratory

UNIVERSITY OF CALIFORNIA

Physics Division

Submitted to Physical Review D

Lepton-Flavor Violation via Right-Handed Neutrino Yukawa Couplings in Supersymmetric Standard Model

J. Hisano, T. Moroi , K. Tobe, and M. Yamaguchi

October 1995

REFERENCE COPY
Does Not
Circulate
Bldg. 50 Library.
LBL-37816
Copy 1

Prepared for the U.S. Department of Energy under Contract Number DE-AC03-76SF00098

DISCLAIMER

This document was prepared as an account of work sponsored by the United States Government. While this document is believed to contain correct information, neither the United States Government nor any agency thereof, nor the Regents of the University of California, nor any of their employees, makes any warranty, express or implied, or assumes any legal responsibility for the accuracy, completeness, or usefulness of any information, apparatus, product, or process disclosed, or represents that its use would not infringe privately owned rights. Reference herein to any specific commercial product, process, or service by its trade name, trademark, manufacturer, or otherwise, does not necessarily constitute or imply its endorsement, recommendation, or favoring by the United States Government or any agency thereof, or the Regents of the University of California. The views and opinions of authors expressed herein do not necessarily state or reflect those of the United States Government or any agency thereof or the Regents of the University of California.

TIT-HEP-304, NSF-ITP-95-127
KEK-TH-450, LBL-37816
UT-727, TU-491
hep-ph/9510309

Lepton-Flavor Violation via Right-Handed Neutrino Yukawa Couplings in Supersymmetric Standard Model *

J. Hisano[(a,b)], T. Moroi[(c,d)], K. Tobe[(e,f)] and M. Yamaguchi[(f)]

[(a)] *Tokyo Institute of Technology, Department of Physics Oh-okayama, Meguro, Tokyo 152, Japan*
[(b)] *Institute for Theoretical Physics, University of California, Santa Barbara, CA 93106, U.S.A.*
[(c)] *Theory Group, KEK, Ibaraki 305, Japan*
[(d)] *Theoretical Physics Group, Lawrence Berkeley Laboratory, University of California, Berkeley, CA 94720, U.S.A.*
[(e)] *Department of Physics, University of Tokyo, Tokyo 113, Japan*
[(f)] *Department of Physics, Tohoku University, Sendai 980-77, Japan*

Abstract

Various lepton-flavor violating (LFV) processes in the supersymmetric standard model with right-handed neutrino supermultiplets are investigated in detail. It is shown that large LFV rates are obtained when $\tan\beta$ is large. In the case where the mixing matrix in the lepton sector has a similar structure as the Kobayashi-Maskawa matrix and the third-generation Yukawa coupling is as large as that of the top quark, the branching ratios can be as large as $Br(\mu \to e\gamma) \simeq 10^{-11}$ and $Br(\tau \to \mu\gamma) \simeq 10^{-7}$, which are within the reach of future experiments. If we assume a large mixing angle solution to the atmospheric neutrino problem, rate for the process $\tau \to \mu\gamma$ becomes larger. We also discuss the difference between our case and the case of the minimal $SU(5)$ grand unified theory.

*This work was supported by the Director, Office of Energy Research, Office of High Energy and Nuclear Physics, Division of High Energy Physics of the U.S. Department of Energy under Contract DE-AC03-76SF00098.

1 Introduction

Lepton-flavor violation (LFV), if observed in a future experiment, is an evidence of new physics beyond the standard model, because the lepton-flavor number is conserved in the standard model. Since the processes do not suffer from a large ambiguity due to the hadronic matrix elements, detailed analysis of the LFV processes will reveal some properties of the high-energy physics.

One of the minimal extensions of the standard model with LFV is the model with non-vanishing neutrino masses. If the masses of the neutrinos are induced by the seesaw mechanism [1], one has a new set of Yukawa couplings involving the right-handed neutrinos. Introduction of the new Yukawa couplings generally gives rise to the flavor violation in the lepton sector, similar to its quark sector counterparts. In non-supersymmetric standard models, however, the amplitudes of the LFV processes are proportional to inverse powers of the right-handed neutrino mass scale which is typically much higher than the electroweak scale, and as a consequence such rates are highly suppressed.

If the model is supersymmetrized, the situation becomes quite different. LFV in the right-handed neutrino Yukawa couplings leads to LFV in slepton masses through renormalization-group effects [2]. Then the LFV processes are only suppressed by powers of supersymmetry (SUSY) breaking scale which is assumed to be at the electroweak scale. Especially, in a previous paper [3], we pointed out that a large left-right mixing of the slepton masses greatly enhances the rates for the LFV processes such as $\mu \to e\gamma$ and $\tau \to \mu\gamma$. Due to this effect, they can be within the reach of near future experiments even if the mixing angle of the lepton sector is as small as that of the quark sector.

In this paper, we will extend the previous analysis. We are interested in the following processes,

- $\mu \to e\gamma$,
- $\tau \to \mu\gamma$,
- $\mu \to eee$,
- μ-e conversion in nuclei,

and calculate formulas for the interaction rates of the above processes. In our calculation, we fully incorporate the mixing of the slepton masses as well as the mixings in the neutralino and chargino sectors. Also the lepton Yukawa couplings in higgsino-lepton-slepton vertices are retained, which yield another type of enhanced diagrams in the large $\tan\beta$

region. Then we will discuss how large the interaction rates can be, assuming the radiative electroweak symmetry breaking scenario [4]. We find that a large value of $\tan\beta$ is realized with relatively light superparticle mass spectrum, and thus the interaction rates can indeed be enhanced. For the right-handed neutrino sector, we will mainly consider the case where the Yukawa couplings of the right-handed neutrinos are similar to those of the up-type quarks. We will also discuss the case of large mixing between the second and third generations, suggested by atmospheric neutrino problem. In our numerical analysis, we impose the constraints from the negative searches for the SUSY particles, as well as the constraint from the muon anomalous-magnetic dipole-moment $g-2$ to which superparticle loops give non-negligible contributions especially in the large $\tan\beta$ region.

The organization of our paper is as follows. In the subsequent section, we will review LFV in slepton masses in the presence of the right-handed neutrinos. In Section 3, we will give formulas of the interaction rates of the various LFV processes. Results of our numerical study are given in Section 4. In Section 5, after summarizing our results, we will compare our case with the case of the $SU(5)$ grand unification briefly. Renormalization-group equations relevant to our analysis are summarized in Appendix A. In Appendix B, we describe the interactions among neutralino (chargino)-fermion-sfermion. In Appendix C, we will give formulas of the SUSY contribution to $g-2$.

2 LFV in scalar lepton masses

Throughout this paper, we consider the minimal SUSY standard model (MSSM) plus three generation right-handed neutrinos. In this case, the superpotential is given by

$$\begin{aligned} W &= f_l^{ij}\epsilon_{\alpha\beta}H_1^\alpha E_i^c L_j^\beta + f_\nu^{ij}\epsilon_{\alpha\beta}H_2^\alpha N_i^c L_j^\beta + f_d^{ij}\epsilon_{\alpha\beta}H_1^\alpha D_i^c Q_j^\beta + f_u^{ij}\epsilon_{\alpha\beta}H_2^\alpha U_i^c Q_j^\beta \\ &\quad + \mu\epsilon_{\alpha\beta}H_1^\alpha H_2^\beta + \frac{1}{2}M_\nu^{ij}N_i^c N_j^c, \end{aligned} \tag{1}$$

where L_i represents the chiral multiplet of a $SU(2)_L$ doublet lepton, E_i^c a $SU(2)_L$ singlet charged lepton, N_i^c a right-handed neutrino which is singlet under the standard-model gauge group, H_1 and H_2 two Higgs doublets with opposite hypercharge. Similarly Q, U and D represent chiral multiplets of quarks of a $SU(2)_L$ doublet and two singlets with different $U(1)_Y$ charges. Three generations of leptons and quarks are assumed and thus the subscripts i and j run over 1 to 3. The symbol $\epsilon_{\alpha\beta}$ is an anti-symmetric tensor with $\epsilon_{12}=1$. The Yukawa interactions are derived from the superpotential via

$$\mathcal{L} = +\frac{1}{2}\sum_{i,j}\frac{\partial^2 W}{\partial\phi_i\partial\phi_j}\psi_i\psi_j + h.c.. \tag{2}$$

SUSY is softly broken in our model. The general soft SUSY breaking terms are given as

$$
\begin{aligned}
-\mathcal{L}_{soft} &= (m_{\tilde{Q}}^2)_i^j \tilde{q}_L^{\dagger i} \tilde{q}_{Lj} + (m_{\tilde{u}}^2)_j^i \tilde{u}_{Ri}^* \tilde{u}_R^j + (m_{\tilde{d}}^2)_j^i \tilde{d}_{Ri}^* \tilde{d}_R^j \\
&+ (m_{\tilde{L}}^2)_i^j \tilde{l}_L^{\dagger i} \tilde{l}_{Lj} + (m_{\tilde{e}}^2)_j^i \tilde{e}_{Ri}^* \tilde{e}_R^j + (m_{\tilde{\nu}}^2)_j^i \tilde{\nu}_{Ri}^* \tilde{\nu}_R^j \\
&+ \tilde{m}_{h1}^2 h_1^\dagger h_1 + \tilde{m}_{h2}^2 h_2^\dagger h_2 + (B\mu h_1 h_2 + \frac{1}{2} B_\nu^{ij} M_\nu^{ij} \tilde{\nu}_{Ri}^* \tilde{\nu}_{Rj}^* + h.c.) \\
&+ (A_d^{ij} h_1 \tilde{d}_{Ri}^* \tilde{q}_{Lj} + A_u^{ij} h_2 \tilde{u}_{Ri}^* \tilde{q}_{Lj} + A_l^{ij} h_1 \tilde{e}_{Ri}^* \tilde{l}_{Lj} + A_\nu^{ij} h_2 \tilde{\nu}_{Ri}^* \tilde{l}_{Lj} \\
&+ \frac{1}{2} M_1 \tilde{B}_L^0 \tilde{B}_L^0 + \frac{1}{2} M_2 \tilde{W}_L^a \tilde{W}_L^a + \frac{1}{2} M_3 \tilde{G}^a \tilde{G}^a + h.c.). \qquad (3)
\end{aligned}
$$

Here the first four lines are soft terms for sleptons, squarks and the Higgs bosons, while the last line gives gaugino mass terms.

We now discuss LFV in the Yukawa couplings. Suppose that the Yukawa coupling matrix f_l^{ij} and the mass matrix of the right-handed neutrinos M_ν^{ij} are diagonalized as $f_{li}\delta^{ij}$ and $M_{Ri}\delta^{ij}$, respectively.[1] Then, in this basis, the neutrino Yukawa couplings f_ν^{ij} are not generally diagonal, giving rise to LFV. An immediate consequence is neutrino oscillation. Writing $f_\nu^{ij} = U^{ik} f_{\nu k} V^{kj}$ with U, V unitary matrices, we obtain the neutrino mass matrix induced by the seesaw mechanism

$$
\begin{aligned}
m_\nu &= f_\nu^{\mathsf{T}} M_\nu^{-1} f_\nu \times \frac{v^2}{2} \sin^2\beta \\
&= V^{\mathsf{T}} \begin{pmatrix} f_{\nu 1} & & \\ & f_{\nu 2} & \\ & & f_{\nu 3} \end{pmatrix} U^{\mathsf{T}} \begin{pmatrix} \frac{1}{M_{R1}} & & \\ & \frac{1}{M_{R2}} & \\ & & \frac{1}{M_{R3}} \end{pmatrix} U \begin{pmatrix} f_{\nu 1} & & \\ & f_{\nu 2} & \\ & & f_{\nu 3} \end{pmatrix} V \\
&\quad \times \frac{v^2}{2} \sin^2\beta, \qquad (4)
\end{aligned}
$$

where $\frac{1}{2}v^2 = \langle h_1 \rangle^2 + \langle h_2 \rangle^2 \simeq (174\mathrm{GeV})^2$ and $\tan\beta = \langle h_2 \rangle / \langle h_1 \rangle$. (Here, $\langle \cdots \rangle$ stands for the vacuum expectation value of the quantity.) Throughout this paper, we assume that M_ν is proportional to the unit matrix $M_\nu^{ij} = M_R \delta^{ij}$, for simplicity. Then, if we disregard possible complex phases in U, the above can be rewritten as

$$
m_\nu = \frac{1}{M_R} V^{\mathsf{T}} \begin{pmatrix} f_{\nu 1}^2 & & \\ & f_{\nu 2}^2 & \\ & & f_{\nu 3}^2 \end{pmatrix} V \times \frac{v^2}{2} \sin^2\beta. \qquad (5)
$$

Thus as far as $V \neq 1$ and the mass eigenvalues are non-degenerate, we have neutrino oscillation which is a target of current and future experiments.

[1] We can always choose f_l^{ij} and M_ν^{ij} to be diagonal by using unitary transformations of L, E^c and N^c.

The smallness of the neutrino masses implies that the scale M_R is very high, $\sim 10^{12}$ GeV or even higher. In the standard model with right-handed neutrinos, the flavor violating processes such as $\mu \to e\gamma$, $\tau \to \mu\gamma$ *etc.*, whose rates are proportional to inverse powers of M_R, would be highly suppressed with such a large M_R scale, and hence those would never be seen experimentally.

However, if there exists SUSY broken at the electroweak scale, we may expect that the rates of these LFV processes will be much larger than the non-supersymmetric case. The point is that the lepton-flavor conservation is not a consequence of the standard-model gauge symmetry and renormalizability in the supersymmetric case, even in the absence of the right-handed neutrinos. Indeed, slepton mass terms can violate the lepton-flavor conservation in a manner consistent with the gauge symmetry. Thus the scale of LFV can be identified with the electroweak scale, much lower than the right-handed neutrino scale M_R. However, an order-of-unity violation of the lepton-flavor conservation at the electroweak scale would cause disastrously large rates for $\mu \to e\gamma$ and others. Also, arbitrary squark masses result in too large rates for various flavor-changing-neutral-current processes involving squark loops. To avoid these problems, one often considers that the sleptons and the squarks are degenerate in masses among those with the same gauge quantum numbers in the tree-level Lagrangian at a certain renormalization scale. In the following, we will assume a somewhat stronger hypothesis that all SUSY breaking scalar masses are universal at the gravitational scale $M \equiv m_{pl}/\sqrt{8\pi} \sim 2 \times 10^{18}$GeV, *i.e.*, we adopt the minimal supergravity type boundary conditions. Thus we will consider the following type of soft terms,

- universal scalar mass (m_0),
  all scalar masses of the type $(m^2_{\tilde{f}})^j_i$ and $\tilde{m}^2_{h_i}$ $(i = 1, 2)$ take common value m_0^2,
- universal A-parameter,
  $A^{ij}_f = a f^{ij}_f m_0$ with a being a constant of order unity,

at the renormalization scale M.[2] As for the gaugino masses, for simplicity, we choose the boundary condition so that they satisfy the so-called grand unified theory (GUT) relation at low energies. Note that the universal scalar masses are given in a certain class of supergravity models with hidden sector SUSY breaking [5]. Those soft SUSY

[2]In fact, there is another SUSY breaking parameter B, which gives a mixing term of the two Higgs bosons h_1 and h_2. For a given value of $\tan\beta$, we fix this parameter B (and also the SUSY invariant Higgs mass μ) so that the Higgs bosons have correct vacuum expectation values, $\langle h_1 \rangle = v\cos\beta/\sqrt{2}$ and $\langle h_2 \rangle = v\sin\beta/\sqrt{2}$.

breaking terms suffer from renormalization via gauge and Yukawa interactions, which can be conveniently expressed in terms of the renormalization-group equations (RGEs). The RGEs relevant in our analysis will be given in Appendix A. An important point is that, through this renormalization effect, LFV in the Yukawa couplings induces LFV in the slepton masses at low energies even if the scalar masses are universal at high energy. Due to this fact, lepton-flavor conservation is violated at low energies.

We can solve the RGEs numerically with the boundary conditions given above. It is, however, instructive to consider here a simple approximation to estimate the LFV contribution to the slepton masses. Since the $SU(2)_L$ doublet lepton multiplets have the lepton-flavor violating Yukawa couplings with the right-handed neutrino multiplets, the LFV effect most directly appears in the mass matrix of the doublet sleptons. The RGEs for them can be written as (see Appendix A)

$$\begin{aligned}\mu\frac{d}{d\mu}(m^2_{\tilde{L}})^j_i &= \left(\mu\frac{d}{d\mu}(m^2_{\tilde{L}})^j_i\right)_{\rm MSSM} \\ &\quad +\frac{1}{16\pi^2}\left[(m^2_{\tilde{L}}f^\dagger_\nu f_\nu + f^\dagger_\nu f_\nu m^2_{\tilde{L}})^j_i + 2(f^\dagger_\nu m^2_{\tilde{\nu}} f_\nu + \tilde{m}^2_{h2} f^\dagger_\nu f_\nu + A^\dagger_\nu A_\nu)^j_i\right]. \quad (6)\end{aligned}$$

Here $(\mu\frac{d}{d\mu}(m^2_{\tilde{L}})^j_i)_{\rm MSSM}$ denotes the RGE in case of the MSSM, and the terms explicitly written are additional contributions by the right-handed neutrino Yukawa couplings. An iteration gives an approximate solution for the additional contributions to the mass terms

$$\begin{aligned}(\Delta m^2_{\tilde{L}})^j_i &\approx -\frac{\ln(M/M_R)}{16\pi^2}\left(6m_0^2(f^\dagger_\nu f_\nu)^j_i + 2(A^\dagger_\nu A_\nu)^j_i\right) \\ &= -\frac{\ln(M/M_R)}{16\pi^2}(6+2a^2)m_0^2(f^\dagger_\nu f_\nu)^j_i, \quad (7)\end{aligned}$$

where we have used the universal scalar mass and A-parameter conditions. In Eq. (7),

$$(f^\dagger_\nu f_\nu)^j_i = f^\dagger_{\nu ik} f^{kj}_\nu = V^*_{ki}|f_{\nu k}|^2 V^{kj}, \quad (8)$$

so that the slepton mass $(m^2_{\tilde{L}})^j_i$ indeed has the generation mixing if V differs from the unit matrix in the basis that the charged lepton Yukawa coupling f_l are diagonal.

Lack of our knowledge on the neutrino Yukawa couplings prevents us from giving a definite prediction of the slepton mass matrix, and thus the rates of the LFV processes. Nevertheless, it is important to study how large the interaction rates for the LFV processes can be for some typical cases and to see whether those signals can be tested by experiments. In this paper, we shall consider the following typical two cases: *case 1*) the mixing matrix V is identical to the Kobayashi-Maskawa (KM) matrix in the quark sector V_{KM}, and *case 2*) the mixing matrix is given so that it can explain atmospheric neutrino

deficit by the large-mixing ν_τ-ν_μ oscillation. In the latter case, we only consider $\tau \to \mu\gamma$, the generation mixing between the second and third ones.

3 Interaction rates for LFV processes

In this section we give formulas of the interaction rates for the LFV processes we consider. Results of our numerical calculation will be given in the next section.

We first explain how the rates for $\mu \to e\gamma$ and $\tau \to \mu\gamma$ can be enhanced compared with the naive expectation when $\tan\beta$ is large. Here, we consider in the basis where the neutralino/chargino interactions to the leptons and the sleptons are flavor diagonal and the effect of the flavor violation in the lepton sector is involved by the mass insertions $(m^2_{\tilde{L}})^j_i$ $(i \neq j)$. First, let us consider contribution from winos and bino, the $SU(2)_L \times U(1)_Y$ gauginos, neglecting the mixing in the chargino/neutralino sector. A naive estimate on the branching ratio yields

$$Br(l_j \to l_i\gamma) \propto \frac{\alpha^3}{G_F^2} \frac{((m^2_{\tilde{L}})^j_i)^2}{m_S^8}, \tag{9}$$

where m_S is the typical mass of superparticles, α the fine structure constant and G_F the Fermi constant. The contribution from Feynman diagrams Fig. 1(a) and (b) follows this estimate. However, as emphasized in our previous paper [3], the diagram Fig. 1(c) which picks up the left-right mixing of the sleptons and exchanges the bino in the loop can give much larger contribution, when $\mu\tan\beta$ is much larger than the masses of the other superparticles. Indeed we estimate the ratio of the amplitudes

$$\frac{Amp.(1.c)}{Amp.(1.a+b)} \sim \frac{M_1 m^2_{LRjj}}{m_{l_j} m_S^2} \sim \frac{\mu\tan\beta}{m_S}\frac{M_1}{m_S}, \tag{10}$$

with m_{l_j} being the charged lepton l_j mass. In Ref. [3], we numerically showed that this enhancement really occurs for the case of large $\mu\tan\beta$.

If we take account of the gaugino-higgsino mixing in the chargino/neutralino sector, we find another type of diagram which enhances the amplitude when $\tan\beta$ is large but μ is comparable to the masses of the other superparticles. It is shown in Fig. 2. In this diagram, one has the mixing between the higgsino and the gaugino which is proportional to $v\sin\beta$, the vacuum expectation value of h_2, and involves the Yukawa coupling of higgsino-lepton-slepton, $f_{l_j} = -\sqrt{2}m_{l_j}/(v\cos\beta)$. The sleptons inside a loop are left-handed ones. Thus the amplitude is proportional to $\tan\beta$, and

$$\frac{Amp.(2)}{Amp.(1.a+b)} \sim \tan\beta. \tag{11}$$

Note that this type of diagram includes neutralino-exchange graphs as well as a chargino-exchange graph.

In this work, we are interested in the following LFV processes; $\mu \to e\gamma$ and $\tau \to \mu\gamma$, $\mu^- \to e^-e^-e^+$ and μ-e conversion in nuclei. To obtain the interaction rates for these processes, we perform full diagonalization of the slepton mass matrices numerically and consider mixing in the chargino and neutralino sectors.

We write the interaction Lagrangian of fermion-sfermion-neutralino as

$$\mathcal{L} = \bar{f}_i(N_{iAX}^{R(f)}P_R + N_{iAX}^{L(f)}P_L)\tilde{\chi}_A^0\tilde{f}_X + h.c.. \tag{12}$$

In this section, f_i ($f = l, \nu, d, u$) represents a fermion in *mass eigenstate* with the generation index i ($i = 1, 2, 3$), and $\tilde{f}_X$ a sfermion in mass eigenstate. The subscript X runs from 1 to 3 for $\tilde{\nu}$ and from 1 to 6 for the other sfermions, $\tilde{l}, \tilde{d}$ and $\tilde{u}$. A neutralino mass eigenstate is denoted by $\tilde{\chi}_A^0$ ($A = 1, \cdots, 4$) and $P_{R,L} = \frac{1}{2}(1 \pm \gamma_5)$. The coefficients $N_{iAX}^{R(f)}$ and $N_{iAX}^{L(f)}$ depend on the mixing matrices of the neutralino sector and of the sfermions. Their explicit forms will be given in Appendix B. Similarly the fermion-sfermion-chargino interaction is written as

$$\begin{aligned}\mathcal{L} \;=\; & \bar{l}_i(C_{iAX}^{R(l)}P_R + C_{iAX}^{L(l)}P_L)\tilde{\chi}_A^-\tilde{\nu}_X \\ & +\bar{\nu}_i(C_{iAX}^{R(\nu)}P_R + C_{iAX}^{L(\nu)}P_L)\tilde{\chi}_A^+\tilde{l}_X \\ & +\bar{d}_i(C_{iAX}^{R(d)}P_R + C_{iAX}^{L(d)}P_L)\tilde{\chi}_A^-\tilde{u}_X \\ & +\bar{u}_i(C_{iAX}^{R(u)}P_R + C_{iAX}^{L(u)}P_L)\tilde{\chi}_A^+\tilde{d}_X + h.c.,\end{aligned} \tag{13}$$

where $\tilde{\chi}_A^-$ ($A = 1, 2$) is a chargino mass eigenstate. The explicit forms of the coefficients can also be found in the Appendix B.

3.1 Effective Lagrangian for LFV processes

As a first step to compute the LFV rates, let us write down the effective interactions (or amplitudes) relevant for our purpose.

3.1.1 $l_j^- \to l_i^-\gamma^*$

The off-shell amplitude for $l_j^- \to l_i^-\gamma^*$ is generally written as

$$T = e\epsilon^{\alpha *}\bar{u}_i(p-q)\left[q^2\gamma_\alpha(A_1^L P_L + A_1^R P_R) + m_{l_j} i\sigma_{\alpha\beta}q^\beta(A_2^L P_L + A_2^R P_R)\right]u_j(p), \tag{14}$$

in the limit of $q \to 0$ with q being the photon momentum. Here, e is the electric charge, ϵ^* the photon polarization vector, u_i (and v_i in the expressions below) the wave function for

(anti-) lepton, and p the momentum of the particle l_j. In the present case, the Feynman diagrams contributing to the above amplitude are depicted by Fig. 3. Each coefficients in the above can be written as a sum of the two terms,

$$A_a^{L,R} = A_a^{(n)L,R} + A_a^{(c)L,R} \quad (a = 1, 2),$$

where $A_a^{(n)L,R}$ and $A_a^{(c)L,R}$ stand for the contributions from the neutralino loops and from the chargino loops, respectively. We calculate them and find that the neutralino contributions are given by

$$\begin{aligned}
A_1^{(n)L} &= \frac{1}{576\pi^2} N_{iAX}^{R(l)} N_{jAX}^{R(l)*} \frac{1}{m_{\tilde{l}_X}^2} \frac{1}{(1-x_{AX})^4} \\
&\quad \times (2 - 9x_{AX} + 18x_{AX}^2 - 11x_{AX}^3 + 6x_{AX}^3 \ln x_{AX}), \qquad (15) \\
A_2^{(n)L} &= \frac{1}{32\pi^2} \frac{1}{m_{\tilde{l}_X}^2} \left[N_{iAX}^{L(l)} N_{jAX}^{L(l)*} \frac{1}{6(1-x_{AX})^4} \right. \\
&\quad \times (1 - 6x_{AX} + 3x_{AX}^2 + 2x_{AX}^3 - 6x_{AX}^2 \ln x_{AX}) \\
&\quad \left. + N_{iAX}^{L(l)} N_{jAX}^{R(l)*} \frac{M_{\tilde{\chi}_A^0}}{m_{l_j}} \frac{1}{(1-x_{AX})^3} (1 - x_{AX}^2 + 2x_{AX} \ln x_{AX}) \right], \qquad (16) \\
A_a^{(n)R} &= A_a^{(n)L}|_{L \leftrightarrow R} \quad (a = 1, 2), \qquad (17)
\end{aligned}$$

where $x_{AX} = M_{\tilde{\chi}_A^0}^2 / m_{\tilde{l}_X}^2$ is the ratio of the neutralino mass squared, $M_{\tilde{\chi}_A^0}^2$, to the charged slepton mass squared, $m_{\tilde{l}_X}^2$. (Summation over the indices A and X are assumed to be understood.) The chargino contributions are

$$\begin{aligned}
A_1^{(c)L} &= -\frac{1}{576\pi^2} C_{iAX}^{R(l)} C_{jAX}^{R(l)*} \frac{1}{m_{\tilde{\nu}_X}^2} \frac{1}{(1-x_{AX})^4} \\
&\quad \times \left\{ 16 - 45x_{AX} + 36x_{AX}^2 - 7x_{AX}^3 + 6(2 - 3x_{AX}) \ln x_{AX} \right\}, \qquad (18) \\
A_2^{(c)L} &= -\frac{1}{32\pi^2} \frac{1}{m_{\tilde{\nu}_X}^2} \left[C_{iAX}^{L(l)} C_{jAX}^{L(l)*} \frac{1}{6(1-x_{AX})^4} \right. \\
&\quad \times (2 + 3x_{AX} - 6x_{AX}^2 + x_{AX}^3 + 6x_{AX} \ln x_{AX}) \\
&\quad \left. + C_{iAX}^{L(l)} C_{jAX}^{R(l)*} \frac{M_{\tilde{\chi}_A^-}}{m_{l_j}} \frac{1}{(1-x_{AX})^3} (-3 + 4x_{AX} - x_{AX}^2 - 2 \ln x_{AX}) \right], \qquad (19) \\
A_a^{(c)R} &= A_a^{(c)L}|_{L \leftrightarrow R} \quad (a = 1, 2). \qquad (20)
\end{aligned}$$

Here, $x_{AX} = M_{\tilde{\chi}_A^-}^2 / m_{\tilde{\nu}_X}^2$, where $M_{\tilde{\chi}_A^-}$ and $m_{\tilde{\nu}_X}$ are the masses for the chargino $\tilde{\chi}_A^-$ and the sneutrino $\tilde{\nu}_X$, respectively.

3.1.2 $l_j^- \to l_i^- \; l_i^- \; l_i^+$

We next consider the process $l_j^- \to l_i^- \; l_i^- \; l_i^+$ (including $\mu^- \to e^- e^- e^+$). The effective amplitude consists of the contributions from the Penguin-type diagrams and from the box-type diagrams. The former contribution can be computed using Eq. (14), with the result

$$\begin{aligned} T_{\gamma-penguin} &= \bar{u}_i(p_1)\left[q^2\gamma_\alpha(A_1^L P_L + A_1^R P_R) + m_{l_j} i\sigma_{\alpha\beta}q^\beta(A_2^L P_L + A_2^R P_R)\right] u_j(p) \\ &\quad \times \frac{e^2}{q^2}\bar{u}_i(p_2)\gamma^\alpha v_i(p_3) - (p_1 \leftrightarrow p_2). \end{aligned} \tag{21}$$

Furthermore, there are the other Penguin-type diagrams in which the Z boson is exchanged as shown in Fig. 4. This amplitude is

$$\begin{aligned} T_{Z-penguin} = \frac{g_Z^2}{m_Z^2}\bar{u}_i(p_1)\gamma^\mu(F_L P_L + F_R P_R)u_j(p)\bar{u}_i(p_2)\gamma^\mu(Z_L^l P_L + Z_R^l P_R)v_i(p_3) \\ -(p_1 \leftrightarrow p_2), \end{aligned} \tag{22}$$

where $F_{L(R)} = F_{L(R)}^{(c)} + F_{L(R)}^{(n)}$. The chargino contribution $F_{L(R)}^{(c)}$ and the neutralino contribution $F_{L(R)}^{(n)}$ are[3]

$$F_L^{(c)} = -\frac{C_{iAX}^{R(l)} C_{jBX}^{R(l)*}}{16\pi^2}\left[\frac{(O_R)_{A2}(O_R)_{B2}}{4}F_{(X,A,B)} - \frac{(O_L)_{A2}(O_L)_{B2}}{2}G_{(X,A,B)}\right], \tag{23}$$

$$F_R^{(c)} = 0, \tag{24}$$

$$F_L^{(n)} = \frac{N_{iAX}^{R(l)} N_{jBX}^{R(l)*}}{16\pi^2}\frac{(O_N)_{A3}(O_N)_{B3} - (O_N)_{A4}(O_N)_{B4}}{2}\left(F_{(X,A,B)} + 2G_{(X,A,B)}\right), \tag{25}$$

$$F_R^{(n)} = -F_L^{(n)}|_{L\leftrightarrow R}. \tag{26}$$

Here, $O_{L,R}$ and O_N are orthogonal matrices to diagonalize the mass matrices of the chargino and neutralino (see Appendix B), and $F_{(X,A,B)}$ and $G_{(X,A,B)}$ are given by

$$F_{(X,A,B)} = \ln x_{AX} + \frac{1}{x_{AX} - x_{BX}}\left(\frac{x_{AX}^2 \ln x_{AX}}{1 - x_{AX}} - \frac{x_{BX}^2 \ln x_{BX}}{1 - x_{BX}}\right), \tag{27}$$

$$G_{(X,A,B)} = \frac{M_{\chi_A} M_{\chi_B}}{m_{\tilde{l}_X}^2}\frac{1}{x_{AX} - x_{BX}}\left(\frac{x_{AX} \ln x_{AX}}{1 - x_{AX}} - \frac{x_{BX} \ln x_{BX}}{1 - x_{BX}}\right). \tag{28}$$

[3]The Penguin-type diagrams of Z boson contributing to the LFV events do not necessarily need to have chirality flip of lepton as $\mu \to e\gamma$. Therefore, the diagrams picking up Yukawa coupling of higgsino-fermion-sfermion can not become the dominant contribution in Z boson Penguin-type diagrams and we neglect them in the above equations.

In these functions, $M_{\tilde{\chi}_A}$ and $m_{\tilde{l}_X}$ denote neutralino mass and charged slepton mass in the neutralino contribution, and chargino mass and sneutrino mass in the chargino contribution. And, in Eq. (22) the coefficient $Z^l_{L(R)}$ denotes Z boson coupling to charged lepton $l_{L(R)}$, that is,

$$Z^l_{L(R)} = T^l_{3L(R)} - Q^l_{em} \sin^2\theta_W, \tag{29}$$

where $T^l_{3L(R)}$ and Q^l_{em} represent weak isospin ($T^l_{3L} = -\frac{1}{2}$, $T^l_{3R} = 0$) and electric charge ($Q^l_{em} = -1$) of $l_{L(R)}$ respectively.

The box-type Feynman diagrams are given in Fig. 5, and we can write their amplitude as

$$\begin{aligned}
T_{box} \;=\;& B^L_1 e^2\ \bar{u}_i(p_1)\gamma^\alpha P_L u_j(p)\ \bar{u}_i(p_2)\gamma_\alpha P_L v_i(p_3) \\
&+B^R_1 e^2\ \bar{u}_i(p_1)\gamma^\alpha P_R u_j(p)\ \bar{u}_i(p_2)\gamma_\alpha P_R v_i(p_3) \\
&+B^L_2 e^2\ \{\bar{u}_i(p_1)\gamma^\alpha P_L u_j(p)\ \bar{u}_i(p_2)\gamma_\alpha P_R v_i(p_3) - (p_1 \leftrightarrow p_2)\} \\
&+B^R_2 e^2\ \{\bar{u}_i(p_1)\gamma^\alpha P_R u_j(p)\ \bar{u}_i(p_2)\gamma_\alpha P_L v_i(p_3) - (p_1 \leftrightarrow p_2)\} \\
&+B^L_3 e^2\ \{\bar{u}_i(p_1) P_L u_j(p)\ \bar{u}_i(p_2) P_L v_i(p_3) - (p_1 \leftrightarrow p_2)\} \\
&+B^R_3 e^2\ \{\bar{u}_i(p_1) P_R u_j(p)\ \bar{u}_i(p_2) P_R v_i(p_3) - (p_1 \leftrightarrow p_2)\} \\
&+B^L_4 e^2\ \{\bar{u}_i(p_1)\sigma_{\mu\nu} P_L u_j(p)\ \bar{u}_i(p_2)\sigma^{\mu\nu} P_L v_i(p_3) - (p_1 \leftrightarrow p_2)\} \\
&+B^R_4 e^2\ \{\bar{u}_i(p_1)\sigma_{\mu\nu} P_R u_j(p)\ \bar{u}_i(p_2)\sigma^{\mu\nu} P_R v_i(p_3) - (p_1 \leftrightarrow p_2)\},
\end{aligned} \tag{30}$$

where

$$B^{L,R}_a = B^{(n)L,R}_a + B^{(c)L,R}_a \qquad (a = 1, \cdots, 4). \tag{31}$$

The first term represents the neutralino contribution, which we find to be

$$\begin{aligned}
e^2 B^{(n)L}_1 \;=\;& \frac{1}{2} J_{4(A,B,X,Y)} N^{R(l)*}_{jAX} N^{R(l)}_{iAY} N^{R(l)*}_{iBY} N^{R(l)}_{iBX} \\
&+ I_{4(A,B,X,Y)} M_{\tilde{\chi}^0_A} M_{\tilde{\chi}^0_B} N^{R(l)*}_{jAX} N^{R(l)*}_{iAY} N^{R(l)}_{iBY} N^{R(l)}_{iBX},
\end{aligned} \tag{32}$$

$$\begin{aligned}
e^2 B^{(n)L}_2 \;=\;& \frac{1}{4} J_{4(A,B,X,Y)} \Big\{ N^{R(l)*}_{jAX} N^{R(l)}_{iAY} N^{L(l)*}_{iBY} N^{L(l)}_{iBX} + N^{R(l)*}_{jAX} N^{L(l)*}_{iAY} N^{R(l)}_{iBY} N^{L(l)}_{iBX} \\
&- N^{R(l)*}_{jAX} N^{L(l)*}_{iAY} N^{L(l)}_{iBY} N^{R(l)}_{iBX} \Big\} \\
&- \frac{1}{2} I_{4(A,B,X,Y)} M_{\tilde{\chi}^0_A} M_{\tilde{\chi}^0_B} N^{R(l)*}_{jAX} N^{L(l)}_{iAY} N^{L(l)*}_{iBY} N^{R(l)}_{iBX},
\end{aligned} \tag{33}$$

$$\begin{aligned}
e^2 B^{(n)L}_3 \;=\;& I_{4(A,B,X,Y)} M_{\tilde{\chi}^0_A} M_{\tilde{\chi}^0_B} \Big\{ N^{R(l)*}_{jAX} N^{L(l)}_{iAY} N^{R(l)*}_{iBY} N^{L(l)}_{iBX} \\
&+ \frac{1}{2} N^{R(l)*}_{jAX} N^{R(l)*}_{iAY} N^{L(l)}_{iBY} N^{L(l)}_{iBX} \Big\},
\end{aligned} \tag{34}$$

$$
\begin{aligned}
e^2 B_4^{(n)L} &= \frac{1}{8} I_{4(A,B,X,Y)} M_{\tilde{\chi}_A^0} M_{\tilde{\chi}_B^0} N_{jAX}^{R(l)*} N_{iAY}^{R(l)*} N_{iBY}^{L(l)} N_{iBX}^{L(l)}, && (35)\\
B_a^{(n)R} &= B_a^{(n)L}|_{L\leftrightarrow R} \qquad (a=1,\cdots,4). && (36)
\end{aligned}
$$

The chargino contribution is

$$
\begin{aligned}
e^2 B_1^{(c)L} &= \frac{1}{2} J_{4(A,B,X,Y)} C_{jAX}^{R(l)*} C_{iAY}^{R(l)} C_{iBY}^{R(l)*} C_{iBX}^{R(l)}, && (37)\\
e^2 B_2^{(c)L} &= \frac{1}{4} J_{4(A,B,X,Y)} C_{jAX}^{R(l)*} C_{iAY}^{R(l)} C_{iBY}^{L(l)*} C_{iBX}^{L(l)} \\
&\quad -\frac{1}{2} I_{4(A,B,X,Y)} M_{\tilde{\chi}_A^-} M_{\tilde{\chi}_B^-} C_{jAX}^{R(l)*} C_{iAY}^{L(l)} C_{iBY}^{L(l)*} C_{iBX}^{R(l)}, && (38)\\
e^2 B_3^{(c)L} &= I_{4(A,B,X,Y)} M_{\tilde{\chi}_A^-} M_{\tilde{\chi}_B^-} C_{jAX}^{R(l)*} C_{iAY}^{L(l)} C_{iBY}^{R(l)*} C_{iBX}^{L(l)}, && (39)\\
B_4^{(c)L} &= 0, && (40)\\
B_a^{(c)R} &= B_a^{(c)L}|_{L\leftrightarrow R} \qquad (a=1,\cdots,4), && (41)
\end{aligned}
$$

where

$$
\begin{aligned}
iJ_{4(A,B,X,Y)} &= \int \frac{d^4k}{(2\pi)^4} \frac{k^2}{(k^2-M_{\tilde{\chi}_A}^2)(k^2-M_{\tilde{\chi}_B}^2)(k^2-m_{\tilde{l}_X}^2)(k^2-m_{\tilde{l}_Y}^2)}, && (42)\\
iI_{4(A,B,X,Y)} &= \int \frac{d^4k}{(2\pi)^4} \frac{1}{(k^2-M_{\tilde{\chi}_A}^2)(k^2-M_{\tilde{\chi}_B}^2)(k^2-m_{\tilde{l}_X}^2)(k^2-m_{\tilde{l}_Y}^2)}. && (43)
\end{aligned}
$$

Here, $M_{\tilde{\chi}_A}$ and $m_{\tilde{l}_X}$ denote neutralino mass and charged slepton mass in the neutralino contribution, and chargino mass and sneutrino mass in the chargino contribution.

3.1.3 μ-e conversion in nuclei

Finally, we give the formulas for the μ-e conversion in nuclei, *i.e.*, the process $(\mu+(A,Z) \to e+(A,Z))$ where Z and A denote the proton and atomic numbers in a nucleus, respectively. The contribution again consists of the Penguin-type diagrams and the box-type diagrams. The box-type Feynman diagrams are depicted in Fig. 6(b) and (c). We give the effective Lagrangian relevant to this process at the quark level. We find that the Penguin-type diagrams give the following terms,

$$
\begin{aligned}
\mathcal{L}_{eff}^{penguin} &= -\frac{e^2}{q^2}\bar{e}\left[q^2\gamma_\alpha(A_1^L P_L + A_1^R P_R) + m_\mu i\sigma_{\alpha\beta}q^\beta(A_2^L P_L + A_2^R P_R)\right]\mu \\
&\quad \times \sum_{q=u,d} Q_{em}^q \bar{q}\gamma^\alpha q \\
&\quad + \frac{g_Z^2}{m_Z^2}\sum_{q=u,d}\frac{Z_L^q + Z_R^q}{2}\bar{q}\gamma_\alpha q\ \bar{e}\gamma^\alpha(F_L P_L + F_R P_R)\mu, && (44)
\end{aligned}
$$

where the first term comes from the Penguin-type diagrams of photon exchange and the second one Z boson exchange. The coefficient Q^q_{em} denotes the electric charge of the quark q and $Z^q_{L(R)}$ is Z boson coupling to the quark $q_{L(R)}$ such as Eq. (29).

The box-type diagrams give

$$\mathcal{L}^{box}_{eff} = e^2 \sum_{q=u,d} \bar{q}\gamma_\alpha q \;\; \bar{e}\gamma^\alpha (D^L_q P_L + D^R_q P_R)\mu, \tag{45}$$

with

$$D^{L,R}_q = D^{(n)L,R}_q + D^{(c)L,R}_q \qquad (q = u, d). \tag{46}$$

The coefficients are calculated to be

$$\begin{aligned} e^2 D^{(n)L}_q &= \frac{1}{8} J_{4(A,B,X,Y)} (N^{R(l)*}_{\mu AX} N^{R(l)}_{eBX} N^{R(q)}_{qAY} N^{R(q)*}_{qBY} - N^{R(l)*}_{\mu AX} N^{R(l)}_{eBX} N^{L(q)*}_{qAY} N^{L(q)}_{qBY}) \\ &\quad - \frac{1}{4} M_{\tilde{\chi}^0_A} M_{\tilde{\chi}^0_B} I_{4(A,B,X,Y)} (N^{R(l)*}_{\mu AX} N^{R(l)}_{eBX} N^{L(q)}_{qAY} N^{L(q)*}_{qBY} \\ &\quad - N^{R(l)*}_{\mu AX} N^{R(l)}_{eBX} N^{R(q)*}_{qAY} N^{R(q)}_{qBY}), \end{aligned} \tag{47}$$

$$D^{(n)R}_q = D^{(n)L}_q|_{L\leftrightarrow R} \qquad (q = u, d), \tag{48}$$

and

$$\begin{aligned} e^2 D^{(c)L}_d &= \frac{1}{8} J_{4(A,B,X,Y)} C^{R(l)*}_{\mu AX} C^{R(l)}_{eBX} C^{R(d)}_{dAY} C^{R(d)*}_{dBY} \\ &\quad - \frac{1}{4} M_{\tilde{\chi}^-_A} M_{\tilde{\chi}^-_B} I_{4(A,B,X,Y)} C^{R(l)*}_{\mu AX} C^{R(l)}_{eBX} C^{L(d)}_{dAY} C^{L(d)*}_{dBY}, \end{aligned} \tag{49}$$

$$\begin{aligned} e^2 D^{(c)L}_u &= -\frac{1}{8} J_{4(A,B,X,Y)} C^{R(l)*}_{\mu AX} C^{R(l)}_{eBX} C^{L(u)*}_{uAY} C^{L(u)}_{uBY} \\ &\quad + \frac{1}{4} M_{\tilde{\chi}^-_A} M_{\tilde{\chi}^-_B} I_{4(A,B,X,Y)} C^{R(l)*}_{\mu AX} C^{R(l)}_{eBX} C^{R(u)*}_{uAY} C^{R(u)}_{uBY}. \end{aligned} \tag{50}$$

Note that we only take account of the vector contributions for the quark currents. The reason is given as follows. In the limit of the low momentum transfer which is appropriate for the present case ($q^2 \simeq -m^2_\mu$), we can treat the hadronic current in the non-relativistic limit. Furthermore, the contributions from the coherent process dominates over the incoherent ones if we concentrate on the relevant process such as $\mu +^{48}_{22}$ Ti $\rightarrow$ $e +^{48}_{22}$ Ti. Then, the matrix element for the μ-e conversion process is dominated by the contribution from the vector currents.

3.2 Decay rates and conversion rate

Now it is straightforward to calculate the decay rates and the conversion rate, using the amplitudes (or the effective Lagrangian) given in the above subsection.

3.2.1 $l_j^- \to l_i^- \gamma$ decay rate

The decay rate for $l_j^- \to l_i^- \gamma$ is easily calculated using the amplitude (14),

$$\Gamma(l_j^- \to l_i^- \gamma) = \frac{e^2}{16\pi} m_{l_j}^5 (|A_2^L|^2 + |A_2^R|^2). \tag{51}$$

3.2.2 $l_j^- \to l_i^- l_i^- l_i^+$ decay rate

Using the expressions for the amplitude, we can calculate the decay rate,

$$\begin{aligned}
\Gamma(l_j^- \to l_i^- l_i^- l_i^+) = & \frac{e^4}{512\pi^3} m_{l_j}^5 \Big[|A_1^L|^2 + |A_1^R|^2 - 2(A_1^L A_2^{R*} + A_2^L A_1^{R*} + h.c.) \\
& + (|A_2^L|^2 + |A_2^R|^2) \left(\frac{16}{3} \ln \frac{m_{l_j}}{2m_{l_i}} - \frac{14}{9} \right) \\
& + \frac{1}{6}(|B_1^L|^2 + |B_1^R|^2) + \frac{1}{3}(|B_2^L|^2 + |B_2^R|^2) + \frac{1}{24}(|B_3^L|^2 + |B_3^R|^2) \\
& + 6(|B_4^L|^2 + |B_4^R|^2) - \frac{1}{2}(B_3^L B_4^{L*} + B_3^R B_4^{R*} + h.c.) \\
& + \frac{1}{3}(A_1^L B_1^{L*} + A_1^R B_1^{R*} + A_1^L B_2^{L*} + A_1^R B_2^{R*} + h.c.) \\
& - \frac{2}{3}(A_2^R B_1^{L*} + A_2^L B_1^{R*} + A_2^L B_2^{R*} + A_2^R B_2^{L*} + h.c.) \\
& + \frac{1}{3} \Big\{ 2(|F_{LL}|^2 + |F_{RR}|^2) + |F_{LR}|^2 + |F_{RL}|^2 \\
& + (B_1^L F_{LL}^* + B_1^R F_{RR}^* + B_2^L F_{LR}^* + B_2^R F_{RL}^* + h.c.) \\
& + 2(A_1^L F_{LL}^* + A_1^R F_{RR}^* + h.c.) + (A_1^L F_{LR}^* + A_1^R F_{RL}^* + h.c.) \\
& - 4(A_2^R F_{LL}^* + A_2^L F_{RR}^* + h.c.) - 2(A_2^L F_{RL}^* + A_2^R F_{LR}^* + h.c.) \Big\} \Big] ,
\end{aligned} \tag{52}$$

where

$$F_{LL} = \frac{F_L Z_L^l}{m_Z^2 \sin^2\theta_W \cos^2\theta_W}, \tag{53}$$

$$F_{RR} = F_{LL}|_{L \leftrightarrow R}, \tag{54}$$

$$F_{LR} = \frac{F_L Z_R^l}{m_Z^2 \sin^2\theta_W \cos^2\theta_W}, \tag{55}$$

$$F_{RL} = F_{LR}|_{L \leftrightarrow R}. \tag{56}$$

Numerically, we find that a Penguin-type contribution involving A_2^L and A_2^R dominates over the other contributions. In the large $\tan\beta$ region, its effect is enhanced due to the same mechanism as in the case of $l_j^- \to l_i^- \gamma$ process. Furthermore, even in the case where

$\tan\beta$ is not so large, the contribution of the Penguin-type diagram dominates over the box contribution, because of the logarithmic term in Eq. (52) which is quite larger than the other terms.[4] Then, the above formula is greatly simplified, and one finds a simple relation

$$\frac{Br(l_j^- \to l_i^- l_i^- l_i^+)}{Br(l_j^- \to l_i \gamma)} \simeq \frac{\alpha}{8\pi}\left(\frac{16}{3}\ln\frac{m_{l_j}}{2m_{l_i}} - \frac{14}{9}\right). \tag{57}$$

3.2.3 μ-e conversion rate ($\mu + (A,Z) \to e + (A,Z)$)

Once we know the effective Lagrangian relevant to this process at the quark level, we can calculate the conversion rate [7],

$$\begin{aligned}\Gamma(\mu \to e) &= 4\alpha^5 \frac{Z_{eff}^4}{Z}|F(q)|^2\, m_\mu^5 \left[|Z(A_1^L - A_2^R) - (2Z+N)\bar{D}_u^L - (Z+2N)\bar{D}_d^L|^2\right. \\ &\quad \left. + |Z(A_1^R - A_2^L) - (2Z+N)\bar{D}_u^R - (Z+2N)\bar{D}_d^R|^2\right], \end{aligned} \tag{58}$$

where

$$\bar{D}_q^L = D_q^L + \frac{Z_L^q + Z_R^q}{2}\frac{F_L}{m_Z^2 \sin^2\theta_W \cos^2\theta_W}, \tag{59}$$

$$\bar{D}_q^R = D_q^L|_{L\leftrightarrow R} \qquad (q = u, d), \tag{60}$$

and Z and N denote the proton and neutron numbers in a nucleus, respectively. Z_{eff} has been determined in [6] and $F(q^2)$ is the nuclear form factor. In ${}^{48}_{22}$Ti, $Z_{eff} = 17.6, F(q^2 \simeq -m_\mu^2) \simeq 0.54$ [7].

4 Results of the Numerical Calculations

In this section, we present results of our numerical analysis.

As was discussed in Section 2, we assume the universal scalar masses. Also for simplicity, we consider the so-called GUT relation among the gaugino masses

$$\frac{M_1}{g_1^2} = \frac{M_2}{g_2^2} = \frac{M_3}{g_3^2}. \tag{61}$$

Then the SUSY breaking terms have four free parameters; the universal scalar mass (m_0), the $SU(2)_L$ gaugino mass at low energies (M_2), the universal A-parameter ($A = am_0$) and mixing parameter of the two Higgs bosons (B).

[4]This logarithmic term is obtained as a result of the phase space integration of the fermions in the final state, since we have an infrared singularity in the limit of $m_{l_i} \to 0$.

Concerning the SUSY invariant Higgs mass μ and B-parameter which parameterize the mixing among h_1 and h_2, we determined them so that the two Higgs doublets have correct vacuum expectation values $\langle h_1 \rangle = v \cos\beta/\sqrt{2}$ and $\langle h_2 \rangle = v \sin\beta/\sqrt{2}$. With this radiative electroweak symmetry breaking condition [4], we determine the mass spectra and mixing matrices of the superparticles. Then, we carefully investigate the parameter space where $\tan\beta$ is large and masses of superparticles (especially, sleptons and electroweak gauginos) are quite light enough to enhance the LFV rates. As a result, we found that there indeed exists parameter space where the above conditions are satisfied. We checked, for $M_2 = 80\text{GeV}$, $\tan\beta$ can be as large as about 50.[5] This result implies that there are regions in the parameter space where the LFV processes have large branching ratios due to the large $\tan\beta$ enhancement mechanism.[6]

We also put constraints from experiments. Besides our requirement that the lightest superparticle be neutral, we use consequences of the negative searches for the superparticles [8]. We also impose a constraint on SUSY contribution to the anomalous magnetic dipole-moment of the muon [11, 12]. The experimental value of $\frac{1}{2}(g-2)$ is $1165923(8.4) \times 10^{-9}$ [8]. On the other hand, the theoretical prediction of standard model is $11659180(15.3) \times 10^{-10}$ or $11659183(7.6) \times 10^{-10}$ [12], where the difference is due to different estimates of hadronic contributions. In our paper, we adopt the first one in order to derive conservative bound. Therefore, the SUSY contribution should be constrained as

$$-26.7 \times 10^{-9} < (g-2)_\mu^{SUSY} < 46.7 \times 10^{-9}, \tag{62}$$

where two sigma experimental error is considered. The SUSY contribution is shown in Fig. 7. Here, we take the parameter $a = 0$ at the gravitational scale and $M_2 = 100$ GeV at low energies. The horizontal line is taken to be the left-handed selectron mass with the D-term contribution, which we denote by $m_{\tilde{e}_L}$. One finds that a significant region of the parameter space is excluded by this constraint in the large $\tan\beta$ region. This is because the same enhancement mechanism as the LFV processes works in the diagrams contributing to the $g-2$. For completeness, we will give formulas of the contribution of the superparticle loops to the anomalous magnetic dipole-moment in Appendix C.

Let us now discuss the branching ratios for each LFV process. First we consider the case where the neutrino mixing matrix is described by the KM matrix.

[5]Throughout this paper, we take the top quark mass $m_t = 174$ GeV [8]. Also we take the bottom quark mass $m_b = 4.25\text{GeV}$ [9], which corresponds to 3.1 GeV at the Z mass scale.

[6]Note that the situation here contrasts to the case of the Yukawa unification where the radiative breaking with the universal scalar mass requires heavy superparticle spectrum, larger than, say, 500 GeV [10].

4.1 *Case 1)* $V = V_{KM}$

As the first trial, we shall consider the case where $V = V_{KM}$, where we take $s_{12} = 0.22$, $s_{23} = 0.04$ and $s_{13} = 0.0035$ in the standard notation [8]. We ignore the possible Kobayashi-Maskawa complex phase and consider V to be real, for simplicity. The eigenvalues of the neutrino Yukawa couplings are assumed to be equal to those of the up-type quarks at the gravitational scale. Since the magnitude of the top quark Yukawa coupling is close to its perturbative bound, this ansatz will maximize the magnitude of LFV in the slepton mass matrix. Also, to determine the right-handed neutrino Majorana mass M_R, we fix the tau neutrino mass at 10 eV so that it constitutes the hot component of the dark matter of the Universe. In this case, M_R is about 10^{12-13} GeV.

Solving the RGEs numerically, we obtain the mass squared matrix for the $SU(2)_L$ doublet sleptons at the electroweak scale

$$m_{\tilde{L}}^2 \simeq \begin{pmatrix} 1.00 & (0.30-0.43)\times 10^{-4} & -(0.74-1.07)\times 10^{-3} \\ (0.30-0.43)\times 10^{-4} & 1.00 & -(0.54-0.78)\times 10^{-2} \\ -(0.74-1.07)\times 10^{-3} & -(0.54-0.78)\times 10^{-2} & 0.77-0.80 \end{pmatrix} \times m_0^2, \tag{63}$$

where $\tan\beta$ varies from 3 to 30, $M_2 = 0$ and $a = 0$. For a non-vanishing M_2, the diagonal elements of the above matrix become larger and the flavor-violating off-diagonal elements become relatively less important, as the gaugino mass gets larger. Effect of non-vanishing a-parameter can be seen from Eq. (7), which does not change the result drastically. In the following numerical calculations we will take $a = 0$.

We find in Eq. (63) the off-diagonal elements in the mass matrix are small. This is because the off-diagonal slepton masses are proportional to $V_{3i}^* V^{3j}$ in the case of hierarchical neutrino masses, which are small if we assume that V is equal to the KM matrix. Nevertheless, as will be shown shortly, the enhancement in the large $\tan\beta$ region yields large branching ratios for the LFV processes, which is close to the present experimental upper bounds.

4.1.1 $\mu \to e\gamma$

Result of our computation on the branching ratio $Br(\mu \to e\gamma)$ is shown in Fig. 8 for $M_2 = 100$ GeV. The horizontal line is taken to be the left-handed selectron mass with the D-term contribution, $m_{\tilde{e}_L}$. Real lines are for $\mu > 0$, while dashed lines for $\mu < 0$. We can find that the branching ratios are rather insensitive to the choice of the sign of the μ-parameter, in particular when $\tan\beta$ is large. For the large $\tan\beta$ case, some regions

of small slepton masses are excluded by the constraint from $g-2$. As can be seen from Fig. 7, it is less stringent for $\mu > 0$ case than $\mu < 0$ case.[7] One can see that even if we impose this constraint, the branching ratio can be as large as 10^{-11}, which is very close to the present experimental bound $Br(\mu \to e\gamma)|_{\rm exp} < 4.9 \times 10^{-11}$. For smaller value of $\tan\beta$, the branching ratio reduces obeying $\propto \tan^2\beta$.

We compared the chargino loop contribution with the neutralino loop contribution and found that the former dominates. This is important when we compare our results with the case of $SU(5)$ grand unification. (See Section 5.)

In Fig. 9, we show the case of $M_2 = 200$ GeV. The maximum of the branching ratio is about 10^{-12} for $\tan\beta = 30$, about one order of magnitude smaller than the $M_2 = 100$ GeV case. We also studied the case $M_2 = 80$ GeV, and found that the branching ratio is about factor 2 larger than the $M_2 = 100$ GeV case.

4.1.2 $\mu^- \to e^-e^-e^+$

Next, let us consider the process $\mu^- \to e^-e^-e^+$. Currently the experimental upper bound on the branching ratio of this process is 1.0×10^{-12} [8]. We show results of our calculation to this process in Fig. 10 for $M_2 = 100$ GeV. The branching ratio has the maximum of $\sim 10^{-13}$ for the large $\tan\beta$ with the small gaugino mass. One can check that this process is dominated by the Penguin-type diagrams. Indeed compared with the branching ratio of $\mu \to e\gamma$, one finds a simple relation

$$\frac{Br(\mu \to 3e)}{Br(\mu \to e\gamma)} \sim 7 \times 10^{-3}, \tag{64}$$

which is in agreement with the ratio expected by the dominance of the Penguin-type diagrams, Eq. (57).

4.1.3 μ-e conversion in $^{48}_{22}$Ti

Experimentally, μ-e conversion rate in nuclei is also constrained strongly. The experimental upper bound on the conversion rate with the target $^{48}_{22}$Ti reaches 4.3×10^{-12} [8].

[7] Here, we should comment that the SUSY contribution to the $b \to s\gamma$ process is also significant and some part of the parameter space should be excluded [12, 13, 14]. However, it is complicated to estimate the SUSY contribution to the $b \to s\gamma$ process, since the chargino loop can contribute either constructively or destructively to the others, especially charged Higgs boson loop. Thus, it seems to us that to determine which regions of the parameter space are really eliminated contains some delicate issues as discussed by Ref. [14]. We believe that such an analysis is out of the scope of our paper, but a work in a future communication. Thus, we do not use the constraint from the $b \to s\gamma$ process.

We show results of our calculation to this process in Fig. 11 for $M_2 = 100$ GeV. The branching ratio takes its maximal value of $\sim 10^{-13}$ in the parameter region where $\tan\beta$ is large and the gaugino masses are small. On the other hand, for the small $\tan\beta$ and $\mu < 0$ the cancelation among the diagrams occurs and the event rate damps rapidly. The Penguin-type diagram is not dominant in the small $\tan\beta$ region because there is not the same logarithmic enhancement as $\mu^- \to e^-e^-e^+$.

4.1.4 $\tau \to \mu\gamma$

Finally we would present our result for $\tau \to \mu\gamma$ in Fig. 12. We find with $M_2 = 100$ GeV, the branching ratio is as large as 10^{-7}, one and a half order of magnitude smaller than the present experimental bound $Br(\tau \to \mu\gamma)|_{\rm exp} < 4.2 \times 10^{-6}$ [8]. Similar to the case of $\mu \to e\gamma$, it can be seen that the branching ratio is proportional to $\tan\beta$ squared.

4.2 *Case 2*) Neutrino mixing implied by atmospheric neutrino deficit

A class of solutions to the atmospheric and solar neutrino deficits requires a maximal mixing of the tau and muon neutrinos, yielding a large off-diagonal element in the slepton mass matrix. The neutrino mixing matrix we take in this example is

$$V \simeq \begin{pmatrix} 1.00 & 0.87 \times 10^{-1} & - \\ -0.66 \times 10^{-1} & 0.755 & 0.656 \\ - & -0.656 & 0.755 \end{pmatrix} \tag{65}$$

and the tau neutrino mass is assumed to be 0.4 eV [15]. Here, we only consider the generation mixing of the second and third generations and ignore the others. The (1,3) and (3,1) elements of the mixing matrix cannot be determined from the solar and atmospheric neutrino deficits. This uncertainty, however, does not matter if we only consider the LFV process among the second and third generations. As in the *case 1*), we assume the magnitude of the third generation neutrino Yukawa coupling $f_{\nu 3}$ is equal to the top quark Yukawa coupling at the gravitational scale. The latter choice will give us a maximum violation of LFV in the slepton mass matrix.

The result for $Br(\tau \to \mu\gamma)$ is shown in Fig. 13. We find that in some portion of the parameter space, the branching ratio exceeds the present experimental upper bound, in particular when $\tan\beta$ is large and the superparticles are light.

5 Conclusions and Discussion

In this paper, we have considered LFV in the minimal supersymmetric standard model (MSSM) with the right-handed neutrino multiplets. In the presence of the Yukawa couplings of the right-handed neutrinos, the left-handed slepton mass matrix, $m_{\tilde{L}}^2$, loses its universal property even if we assume the minimal supergravity type boundary condition on sfermion masses. In our case, due to the renormalization effect, as can be seen from Eq. (63), we obtain LFV in $m_{\tilde{L}}^2$ as well as smaller value of (3,3) element of $m_{\tilde{L}}^2$ compared with the other diagonal elements, which is typical feature of the case with right-handed neutrino [16]. We have calculated the interaction rates for the various LFV processes with the full diagonalization of the slepton mass matrices and of the chargino and neutralino mass matrices. We emphasized the enhancement of the interaction rates for large $\tan\beta$, the ratio of the VEVs of the two Higgs doublets. This enhancement is originated to the fact that there is a freedom to pick up one of two vacuum expectation values in the MSSM in the magnetic dipole-moment type diagrams. For example, for the process $l_j \to l_i\gamma$, the diagrams of the type Fig. 1(c) and Fig. 2 give the enhancement. Even when the mixing matrix in the lepton sector has a similar structure as the KM-matrix of the quark sector, the enhancement mechanism can make the branching ratios close to the present experimental bounds.

It is interesting to compare the LFV processes induced by the right-handed neutrino Yukawa couplings with those in the minimal $SU(5)$ grand unified theory [17, 18]. In the latter case, the renormalization-group flow above the GUT scale results in LFV in the $SU(2)_L$ singlet (right-handed) slepton masses. Let us consider, for example, the resulting branching ratio of $\mu \to e\gamma$. The diagrams which will give the enhancement in the large $\tan\beta$ region are similar to Fig. 1(c) and 2(a). The important difference from the previous case is on Fig. 2. Now, only the diagrams involving the bino contributes, since the wino does not couple to the singlet sleptons. In this case, we can see that contributions coming from the two diagrams Fig. 1(c) and Fig. 2(a) have opposite signs, and thus partially cancel out with each other. Numerical result is shown in Fig. 14. The horizontal line is the mass of the right-handed selectron with the D-term contribution, $m_{\tilde{e}_R}$. Here, we have taken $M_2 = 100$ GeV. The branching ratio never exceeds 10^{-13}, more than two orders of magnitude beneath the present experimental upper bound. Also one finds regions where the branching ratio becomes very small due to the cancelation explained above.

What happens if the standard model with the right-handed neutrinos is embedded in the framework of $SU(5)$ GUT? In this case, both the mass matrix of the left-handed

sleptons and that of the right-handed ones have LFV. The situation is quite similar to the case of $SO(10)$ GUT [18, 19]. For example, if we consider the $\mu \to e\gamma$, the dominant diagram will be similar to Fig. 1(c), which however picks up $(m^2_{LR})^3_3$, proportional to tau-lepton mass. Thus we expect further enhancement in the branching ratio by $(m_\tau/m_\mu)^2$ compared to the case we studied in this paper.

To conclude our paper, we should emphasize that the branching ratios of the LFV processes induced by the right-handed neutrino Yukawa couplings can be close to the present experimental bounds and can be within the reach of future experiments. Efforts of searching for these LFV signals should be encouraged.

Acknowledgment

We would like to thank T. Yanagida for useful discussions. We are also grateful to T. Goto and P. Nath for discussion on the $b \to s\gamma$ process, and to S. Orito for a comment on the anomalous magnetic dipole-moment of the muon. One of authors (J.H.) is a fellow of the Japan Society for the Promotion of Science.

A Renormalization Group Equations

In this appendix, we give the one-loop renormalization group equations (RGEs) for the Yukawa couplings and the soft SUSY breaking terms in the scalar potential. The RGEs for the gauge coupling constants and the gaugino masses are unchanged at the one-loop level, since the right-handed neutrinos are singlet under the standard-model gauge symmetry.

- Yukawa coupling constants

$$\begin{aligned}
\mu\frac{d}{d\mu}f_l^{ij} &= \frac{1}{16\pi^2}\left[\left\{-\frac{9}{5}g_1^2 - 3g_2^2 + 3Tr(f_d f_d^\dagger) + Tr(f_l f_l^\dagger)\right\} f_l^{ij}\right. \\
&\quad \left. +3(f_l f_l^\dagger f_l)^{ij} + (f_l f_\nu^\dagger f_\nu)^{ij}\right], \qquad (66)\\
\mu\frac{d}{d\mu}f_\nu^{ij} &= \frac{1}{16\pi^2}\left[\left\{-\frac{3}{5}g_1^2 - 3g_2^2 + 3Tr(f_u f_u^\dagger) + Tr(f_\nu f_\nu^\dagger)\right\} f_\nu^{ij}\right. \\
&\quad \left. +3(f_\nu f_\nu^\dagger f_\nu)^{ij} + (f_\nu f_l^\dagger f_l)^{ij}\right]. \qquad (67)
\end{aligned}$$

- Soft breaking terms

$$\mu\frac{d}{d\mu}(m^2_{\tilde{L}})^j_i = \frac{1}{16\pi^2}\left[\left(m^2_{\tilde{L}} f_l^\dagger f_l + f_l^\dagger f_l m^2_{\tilde{L}}\right)^j_i + \left(m^2_{\tilde{L}} f_\nu^\dagger f_\nu + f_\nu^\dagger f_\nu m^2_{\tilde{L}}\right)^j_i\right.$$

$$
\begin{aligned}
& +2\left(f_l^\dagger m_{\tilde{e}}^2 f_l + \tilde{m}_{h1}^2 f_l^\dagger f_l + A_l^\dagger A_l\right)_i^j \\
& +2\left(f_\nu^\dagger m_{\tilde{\nu}}^2 f_\nu + \tilde{m}_{h2}^2 f_\nu^\dagger f_\nu + A_\nu^\dagger A_\nu\right)_i^j \\
& -\left(\frac{6}{5}g_1^2\left|M_1\right|^2 + 6g_2^2\left|M_2\right|^2\right)\delta_i^j - \frac{3}{5}g_1^2 S\delta_i^j\Big], \qquad (68)
\end{aligned}
$$

$$
\begin{aligned}
\mu\frac{d}{d\mu}(m_{\tilde{e}}^2)_j^i &= \frac{1}{16\pi^2}\Big[2\left(m_{\tilde{e}}^2 f_l f_l^\dagger + f_l f_l^\dagger m_{\tilde{e}}^2\right)_j^i \\
& +4\left(f_l m_{\tilde{L}}^2 f_l^\dagger + \tilde{m}_{h1}^2 f_l f_l^\dagger + A_l A_l^\dagger\right)_j^i \\
& -\frac{24}{5}g_1^2\left|M_1\right|^2\delta_j^i + \frac{6}{5}g_1^2 S\delta_j^i\Big],
\end{aligned}
$$

$$
\begin{aligned}
\mu\frac{d}{d\mu}(m_{\tilde{\nu}}^2)_j^i &= \frac{1}{16\pi^2}\Big[2\left(m_{\tilde{\nu}}^2 f_\nu f_\nu^\dagger + f_\nu f_\nu^\dagger m_{\tilde{\nu}}^2\right)_j^i \\
& +4\left(f_\nu m_{\tilde{L}}^2 f_\nu^\dagger + \tilde{m}_{h2}^2 f_\nu f_\nu^\dagger + A_\nu A_\nu^\dagger\right)_j^i\Big], \qquad (69)
\end{aligned}
$$

$$
\begin{aligned}
\mu\frac{d}{d\mu}A_l^{ij} &= \frac{1}{16\pi^2}\Big[\Big\{-\frac{9}{5}g_1^2 - 3g_2^2 + 3Tr(f_d^\dagger f_d) + Tr(f_l^\dagger f_l)\Big\}A_l^{ij} \\
& +2\Big\{-\frac{9}{5}g_1^2 M_1 - 3g_2^2 M_2 + 3Tr(f_d^\dagger A_d) + Tr(f_l^\dagger A_l)\Big\}f_l^{ij} \\
& +4(f_l f_l^\dagger A_l)^{ij} + 5(A_l f_l^\dagger f_l)^{ij} + 2(f_l f_\nu^\dagger A_\nu)^{ij} + (A_l f_\nu^\dagger f_\nu)^{ij}\Big], \qquad (70)
\end{aligned}
$$

$$
\begin{aligned}
\mu\frac{d}{d\mu}A_\nu^{ij} &= \frac{1}{16\pi^2}\Big[\Big\{-\frac{3}{5}g_1^2 - 3g_2^2 + 3Tr(f_u^\dagger f_u) + Tr(f_\nu^\dagger f_\nu)\Big\}A_\nu^{ij} \\
& +2\Big\{-\frac{3}{5}g_1^2 M_1 - 3g_2^2 M_2 + 3Tr(f_u^\dagger A_u) + Tr(f_\nu^\dagger A_\nu)\Big\}f_\nu^{ij} \\
& +4(f_\nu f_\nu^\dagger A_\nu)^{ij} + 5(A_\nu f_\nu^\dagger f_\nu)^{ij} + 2(f_\nu f_l^\dagger A_l)^{ij} + (A_\nu f_l^\dagger f_l)^{ij}\Big], \qquad (71)
\end{aligned}
$$

where

$$
S = Tr(m_{\tilde{Q}}^2 + m_{\tilde{d}}^2 - 2m_{\tilde{u}} - m_{\tilde{L}}^2 + m_{\tilde{e}}^2) - \tilde{m}_{h1}^2 + \tilde{m}_{h2}^2. \qquad (72)
$$

Here, we followed the GUT convention for the normalization of $U(1)_Y$ gauge coupling constant g_1, such as $g_Y^2 = \frac{3}{5}g_1^2$.

B Interaction of gaugino-sfermion-fermion

In this appendix, we give our notations and conventions adopted in Section 3 and give vertices relevant for our calculation.

Let us first discuss fermions. We denote by l_i, u_i and d_i the fermion mass eigenstates with the obvious meaning. The subscript i ($i = 1, 2, 3$) represents the generation. As for

the neutrinos, their masses are small and negligible. In our convention, ν_i is the $SU(2)_L$ isodoublet partner to e_{Li}.

Next we consider sfermions. Let $\tilde{f}_{Li}$ and $\tilde{f}_{Ri}$ be the superpartners of f_{Li} and f_{Ri}, respectively. Here, f stands for l, u or d. The mass matrix for the sfermions can be written in the following form,

$$\left(\tilde{f}_L^\dagger, \tilde{f}_R^\dagger\right) \begin{pmatrix} m_L^2 & m_{LR}^{2\mathsf{T}} \\ m_{LR}^2 & m_R^2 \end{pmatrix} \begin{pmatrix} \tilde{f}_L \\ \tilde{f}_R \end{pmatrix}, \tag{73}$$

where m_L^2 and m_R^2 are 3×3 hermitian matrices and m_{LR}^2 is a 3×3 matrix. These elements are given from Eqs. (1,3) as following,

$$m_L^2 = m_{\tilde{f}_L}^2 + m_f^2 + m_Z^2 \cos 2\beta (T_{3L}^f - Q_{em}^f \sin^2\theta_W), \tag{74}$$

$$m_R^2 = m_{\tilde{f}_R}^2 + m_f^2 - m_Z^2 \cos 2\beta (T_{3R}^f - Q_{em}^f \sin^2\theta_W), \tag{75}$$

$$m_{LR}^2 = \begin{cases} -A_f v \sin\beta/\sqrt{2} - m_f \mu \cot\beta & (f = u), \\ A_f v \cos\beta/\sqrt{2} - m_f \mu \tan\beta & (f = d, l), \end{cases} \tag{76}$$

where $T_{3L(R)}^f$ and Q_{em}^f are weak isospin and electric charge respectively. Here, $m_{\tilde{f}_L}^2 = m_{\tilde{Q}}^2$ for squarks, $m_{\tilde{f}_L}^2 = m_{\tilde{L}}^2$ for sleptons, and $m_{\tilde{f}_R}^2$ are each right-handed sfermion soft-breaking masses. We assume the above mass matrix to be real. This is, in general, not diagonal and include mixing between different generations. We diagonalize the mass matrix $\mathcal{M}^2$ by a 6×6 real orthogonal matrix U^f as

$$U^f \mathcal{M}^2 U^{f\mathsf{T}} = (\text{diagonal}), \tag{77}$$

and we denote its eigenvalues by $m_{\tilde{f}_X}^2$ $(X = 1, \cdots, 6)$. The mass eigenstate is then written as

$$\tilde{f}_X = U_{X,i}^f \tilde{f}_{Li} + U_{X,i+3}^f \tilde{f}_{Ri}, \qquad (X = 1, \cdots, 6). \tag{78}$$

Conversely, we have

$$\tilde{f}_{Li} = U_{iX}^{f\mathsf{T}} \tilde{f}_X = U_{Xi}^f \tilde{f}_X, \tag{79}$$

$$\tilde{f}_{Ri} = U_{i+3,X}^{f\mathsf{T}} \tilde{f}_X = U_{X,i+3}^f \tilde{f}_X. \tag{80}$$

An attention should be paid to the neutrinos since there is no right-handed sneutrino in the MSSM. Let $\tilde{\nu}_{Li}$ be the superpartner of the neutrino ν_i. The mass eigenstate $\tilde{\nu}_X$ $(X = 1, 2, 3)$ is related to $\tilde{\nu}_{Li}$ as

$$\tilde{\nu}_{Li} = U_{Xi}^\nu \tilde{\nu}_X. \tag{81}$$

We now turn to charginos. The mass matrix of the charginos is given by

$$-\mathcal{L}_m = \left(\overline{\tilde{W}_R^-}\ \overline{\tilde{H}_{2R}^-}\right) \begin{pmatrix} M_2 & \sqrt{2}m_W \cos\beta \\ \sqrt{2}m_W \sin\beta & \mu \end{pmatrix} \begin{pmatrix} \tilde{W}_L^- \\ \tilde{H}_{1L}^- \end{pmatrix} + h.c.. \tag{82}$$

This matrix M_C is diagonalized by 2×2 real orthogonal matrices O_L and O_R as

$$O_R M_C O_L^{\mathsf{T}} = (\text{diagonal}). \tag{83}$$

Define

$$\begin{pmatrix} \tilde{\chi}_{1L}^- \\ \tilde{\chi}_{2L}^- \end{pmatrix} = O_L \begin{pmatrix} \tilde{W}_L^- \\ \tilde{H}_{1L}^- \end{pmatrix}, \qquad \begin{pmatrix} \tilde{\chi}_{1R}^- \\ \tilde{\chi}_{2R}^- \end{pmatrix} = O_R \begin{pmatrix} \tilde{W}_R^- \\ \tilde{H}_{2R}^- \end{pmatrix}. \tag{84}$$

Then

$$\tilde{\chi}_A^- = \tilde{\chi}_{AL}^- + \tilde{\chi}_{AR}^- \qquad (A = 1, 2) \tag{85}$$

forms a Dirac fermion with mass $M_{\tilde{\chi}_A^-}$.

Finally we consider neutralinos. The mass matrix of the neutralino sector is given by

$$-\mathcal{L}_m = \frac{1}{2}\left(\tilde{B}_L \tilde{W}_L^0 \tilde{H}_{1L}^0 \tilde{H}_{2L}^0\right) M_N \begin{pmatrix} \tilde{B}_L \\ \tilde{W}_L^0 \\ \tilde{H}_{1L}^0 \\ \tilde{H}_{2L}^0 \end{pmatrix} + h.c., \tag{86}$$

where

$$M_N = \begin{pmatrix} M_1 & 0 & -m_Z \sin\theta_W \cos\beta & m_Z \sin\theta_W \sin\beta \\ 0 & M_2 & m_Z \cos\theta_W \cos\beta & -m_Z \cos\theta_W \sin\beta \\ -m_Z \sin\theta_W \cos\beta & m_Z \cos\theta_W \cos\beta & 0 & -\mu \\ m_Z \sin\theta_W \sin\beta & -m_Z \cos\theta_W \sin\beta & -\mu & 0 \end{pmatrix}. \tag{87}$$

The diagonalization is done by a real orthogonal matrix O_N,

$$O_N M_N O_N^{\mathsf{T}} = \text{diagonal}. \tag{88}$$

The mass eigenstates are given by

$$\tilde{\chi}_{AL}^0 = (O_N)_{AB} \tilde{X}_{BL}^0 \qquad (A, B = 1, \cdots, 4) \tag{89}$$

where

$$\tilde{X}_{AL}^0 = (\tilde{B}_L, \tilde{W}_L^0, \tilde{H}_{1L}^0, \tilde{H}_{2L}^0). \tag{90}$$

We have thus Majorana spinors

$$\tilde{\chi}^0_A = \tilde{\chi}^0_{AL} + \tilde{\chi}^0_{AR}, \quad (A = 1, \cdots, 4) \tag{91}$$

with mass $M_{\tilde{\chi}^0_A}$.

We now give the interaction Lagrangian of fermion-sfermion-chargino,

$$\begin{aligned}
\mathcal{L}_{\rm int} &= \bar{l}_i(C^{R(l)}_{iAX}P_R + C^{L(l)}_{iAX}P_L)\tilde{\chi}^-_A\tilde{\nu}_X \\
&\quad +\bar{\nu}_i(C^{R(\nu)}_{iAX}P_R + C^{L(\nu)}_{iAX}P_L)\tilde{\chi}^+_A\tilde{l}_X \\
&\quad +\bar{d}_i(C^{R(d)}_{iAX}P_R + C^{L(d)}_{iAX}P_L)\tilde{\chi}^-_A\tilde{u}_X \\
&\quad +\bar{u}_i(C^{R(u)}_{iAX}P_R + C^{L(u)}_{iAX}P_L)\tilde{\chi}^+_A\tilde{d}_X + h.c.,
\end{aligned} \tag{92}$$

where the coefficients are

$$\begin{aligned}
C^{R(l)}_{iAX} &= -g_2(O_R)_{A1}U^{\nu}_{X,i}, \\
C^{L(l)}_{iAX} &= g_2\frac{m_{l_i}}{\sqrt{2}m_W\cos\beta}(O_L)_{A2}U^{\nu}_{X,i}, \\
C^{R(\nu)}_{iAX} &= -g_2(O_L)_{A1}U^{l}_{X,i}, \\
C^{L(\nu)}_{iAX} &= g_2\frac{m_{l_i}}{\sqrt{2}m_W\cos\beta}(O_L)_{A2}U^{l}_{X,i+3}, \\
C^{R(d)}_{iAX} &= g_2\{-(O_R)_{A1}U^{u}_{Xi} + \frac{m_{u_i}}{\sqrt{2}m_W\sin\beta}(O_R)_{A2}U^{u}_{X,i+3}\}, \\
C^{L(d)}_{iAX} &= g_2\frac{m_{d_i}}{\sqrt{2}m_W\cos\beta}(O_L)_{A2}U^{u}_{X,i}, \\
C^{R(u)}_{iAX} &= g_2\{-(O_L)_{A1}U^{d}_{X,i} + \frac{m_{d_i}}{\sqrt{2}m_W\cos\beta}(O_L)_{A2}U^{d}_{X,i+3}\}, \\
C^{L(u)}_{iAX} &= g_2\frac{m_{u_i}}{\sqrt{2}m_W\sin\beta}(O_R)_{A2}U^{d}_{X,i}.
\end{aligned} \tag{93}$$

The interaction Lagrangian of fermion-sfermion-neutralino is similarly written as

$$\mathcal{L}_{\rm int} = \bar{f}_i(N^{R(f)}_{iAX}P_R + N^{L(f)}_{iAX}P_L)\tilde{\chi}^0_A\tilde{f}_X \tag{94}$$

where f stands for l, ν, d and u. The coefficients are

$$\begin{aligned}
N^{R(l)}_{iAX} &= -\frac{g_2}{\sqrt{2}}\{[-(O_N)_{A2} - (O_N)_{A1}\tan\theta_W]U^{l}_{X,i} + \frac{m_{l_i}}{m_W\cos\beta}(O_N)_{A3}U^{l}_{X,i+3}\}, \\
N^{L(l)}_{iAX} &= -\frac{g_2}{\sqrt{2}}\{\frac{m_{l_i}}{m_W\cos\beta}(O_N)_{A3}U^{l}_{x,i} + 2(O_N)_{A1}\tan\theta_W U^{l}_{X,i+3}\}, \\
N^{R(\nu)}_{iAX} &= -\frac{g_2}{\sqrt{2}}[(O_N)_{A2} - (O_N)_{A1}\tan\theta_W]U^{\nu}_{X,i}, \\
N^{L(\nu)}_{iAX} &= 0,
\end{aligned}$$

$$
\begin{aligned}
N_{iAX}^{R(d)} &= -\frac{g_2}{\sqrt{2}}\{[-(O_N)_{A2}+\frac{1}{3}(O_N)_{A1}\tan\theta_W]U_{X,i}^d+\frac{m_{d_i}}{m_W\cos\beta}(O_N)_{A3}U_{X,i+3}^d\},\\
N_{iAX}^{L(d)} &= -\frac{g_2}{\sqrt{2}}\{\frac{m_{d_i}}{m_W\cos\beta}(O_N)_{A3}U_{X,i}^d+\frac{2}{3}\tan\theta_W(O_N)_{A1}U_{X,i+3}^d\},\\
N_{iAX}^{R(u)} &= -\frac{g_2}{\sqrt{2}}\{[(O_N)_{A2}+\frac{1}{3}(O_N)_{A1}\tan\theta_W]U_{X,i}^u+\frac{m_{u_i}}{m_W\sin\beta}(O_N)_{A4}U_{X,i+3}^u\},\\
N_{iAX}^{L(u)} &= -\frac{g_2}{\sqrt{2}}\{\frac{m_{u_i}}{m_W\sin\beta}(O_N)_{A4}U_{X,i}^u-\frac{4}{3}\tan\theta_W(O_N)_{A1}U_{X,i+3}^u\}. \qquad (95)
\end{aligned}
$$

C Anomalous magnetic dipole-moment of the muon

The magnetic dipole-moment interaction of muon is written as the following form;

$$
\frac{ie}{2m_\mu}F(q^2)\bar{u}(p_f)\sigma_{\mu\nu}q^\mu\epsilon^\nu u(p_i), \qquad (96)
$$

where $q=p_f-p_i$ and ϵ the polarization vector of external photon. Then, the anomalous magnetic dipole-moment of muon is

$$
(g-2)_\mu \equiv 2F(q^2=0). \qquad (97)
$$

We can write SUSY contributions as $(g-2)_\mu^{SUSY}=(g^{(C)}+g^{(N)})_\mu$. The first term $g_\mu^{(C)}$ represents the chargino-loop contribution as

$$
\begin{aligned}
g_\mu^{(C)} &= \frac{1}{48\pi^2}\frac{m_\mu^2}{m_{\tilde{\nu}_X}^2}|C_{2AX}^{L(l)}|^2\frac{2+3x_{AX}-6x_{AX}^2+x_{AX}^3+6x_{AX}\ln x_{AX}}{(1-x_{AX})^4}\\
&+\frac{1}{16\pi^2}\frac{m_\mu M_{\tilde{\chi}_A^-}}{m_{\tilde{\nu}_X}^2}C_{2AX}^{L(l)}C_{2AX}^{R(l)*}\frac{-3+4x_{AX}-x_{AX}^2-2\ln x_{AX}}{(1-x_{AX})^3}\\
&+(L\leftrightarrow R) \qquad (98)
\end{aligned}
$$

where $x_{AX}=M_{\tilde{\chi}_A^-}^2/m_{\tilde{\nu}_X}^2$.

The neutralino-loop contribution $g_\mu^{(N)}$ is

$$
\begin{aligned}
g_\mu^{(N)} &= -\frac{1}{48\pi^2}\frac{m_\mu^2}{m_{\tilde{l}_X}^2}|N_{2AX}^{L(l)}|^2\frac{1-6x_{AX}+3x_{AX}^2+2x_{AX}^3-6x_{AX}^2\ln x_{AX}}{(1-x_{AX})^4}\\
&-\frac{1}{16\pi^2}\frac{m_\mu M_{\tilde{\chi}_A^0}}{m_{\tilde{l}_X}^2}N_{2AX}^{L(l)}N_{2AX}^{R(l)*}\frac{1-x_{AX}^2+2x_{AX}\ln x_{AX}}{(1-x_{AX})^3}\\
&+(L\leftrightarrow R), \qquad (99)
\end{aligned}
$$

where $x_{AX}=M_{\tilde{\chi}_A^0}^2/m_{\tilde{l}_X}^2$.

References

[1] T. Yanagida, in *Proceedings of the Workshop on Unified Theory and Baryon Number of the Universe*, eds. O. Sawada and A. Sugamoto (KEK, 1979) p.95;
M. Gell-Mann, P. Ramond and R. Slansky, in *Supergravity*, eds. P. van Niewwenhuizen and D. Freedman (North Holland, Amsterdam, 1979).

[2] F. Borzumati and A. Masiero, *Phys. Rev. Lett.* **57** (1986) 961.

[3] J. Hisano, T. Moroi, K. Tobe, M. Yamaguchi and T. Yanagida, *Phys. Lett.* **B357** (1995) 579.

[4] K. Inoue, A. Kakuto, H. Komatsu and S. Takeshita, *Prog. Theor. Phys.* **68** (1982) 927.

[5] For review, H.P. Nilles, *Phys. Rep.* **110** (1984) 1.

[6] J. C. Sen, *Phys. Rev.* **113** (1959) 679;
K. W. Ford and J. G. Wills, *Nucl. Phys.* **35** (1962) 295;
R. Pla and J. Bernabéu, *An. Fis.* **67** (1971) 455;
H. C. Chiang, E. Oset, T. S. Kosmas, A. Faessler and J. D. Vergados, *Nucl. Phys.* **A559** (1993) 526.

[7] J. Bernabeu, E. Nardi and D. Tommasini, *Nucl. Phys.* **B409** (1993) 69, and reference there in.

[8] L. Montanet *et al.* (Particle Data Group), *Phys. Rev.* **D50** (1994) 1173.

[9] J. Gasser and H. Leutwyler, *Phys. Rep.* **C87** (1982) 77.

[10] M. Bando, T. Kugo, N. Maekawa and H. Nakano, *Mod. Phys. Lett.* **A7** (1992) 3379.

[11] D.A. Kosower, L.M. Krauss and N. Sakai, *Phys. Lett.* **B133** (1983) 305;
T.C. Yuan, R. Arnowitt, A.H. Chamseddine and P. Nath, *Z. Phys.* **C26** (1984) 407.

[12] U. Chattopadhyay and P. Nath, preprint NSF-ITP-95-64 (hep-ph/9507386), and reference there in.

[13] J.L. Lopez, D.V. Nanopoulos, X. Wang and A. Zichichi, *Phys. Rev.* **D51** (1995) 147;
T. Goto and Y. Okada, *Prog. Theor. Phys.* **94** (1995) 407;
Kraniotis, preprint SUSX-TH-95-15 (hep-ph/9507432).

[14] B. de Carlos and J.A. Casas, *Phys. Lett.* **B300** (1995) 300; *ERRATUM-ibid* **B351** (1995) 604.

[15] J.G. Learned, S. Pakvasa and T.J. Weiler, *Phys. Lett.* **B207** (1988) 79.

[16] T. Moroi, *Phys. Lett.* **B321** (1994) 56.

[17] R. Barbieri and L.J. Hall, *Phys. Lett.* **B338** (1994) 212.

[18] R. Barbieri, L.J. Hall and A. Strumia, *Nucl. Phys.* **B445** (1995) 219.

[19] P. Ciafaloni, A. Romanino and A. Strumia, preprint IFUP-TH-42-95 (hep-ph/9507379);
N. Arkani-Hamed, S.-C. Cheng and L.J. Hall, preprint LBL-37343 (hep-ph/9508288).

Figure Caption

Fig. 1

Feynman diagrams which give rise to $l_j \to l_i\gamma$. The symbols $\tilde{e}_{Li}$, $\tilde{\nu}_{Li}$, $\tilde{B}$, $\tilde{W}^0$, and $\tilde{W}^-$ represent left-handed charged sleptons, left-handed sneutrinos, bino, neutral wino, and charged wino, respectively. In (a) and (b), the blob in the the slepton/sneutrino line indicates the flavor-violating mass insertion of the left-handed slepton and another blob in the external line the chirality flip of the external lepton l_j. In (c), the blobs in the slepton line indicate the insertions of the flavor-violating mass ($m^{2\,j}_{\tilde{L}i}$) and the left-right mixing mass (m^2_{LRjj}), and another blob in the bino line the chirality flip of the bino $\tilde{B}$.

Fig.2

Feynman diagrams which give rise to the large $\tan\beta$ enhancement due to the gaugino-higgsino mixing in the process of $l_j \to l_i\gamma$. The symbols $\tilde{e}_{Li}$, $\tilde{\nu}_{Li}$, $\tilde{B}$, $\tilde{W}^0$, $\tilde{W}^-$, $\tilde{H}^0$, and $\tilde{H}^-$ represent left-handed charged sleptons, left-handed sneutrinos, bino, neutral wino, charged wino, neutral higgsino, and charged higgsino, respectively. The blob in the slepton/sneutrino line indicates the insertion of the flavor-violating mass ($m^{2\,j}_{\tilde{L}i}$). The blobs in the gaugino-higgsino line indicate the mass insertions for gaugino-higgsino mixing, that is, μ denotes higgsino ($\tilde{H}_1$-$\tilde{H}_2$) mass mixing, $v\sin\beta$ the gaugino-higgsino ($\tilde{H}_2$-$\tilde{W}$) mass mixing, and M_2 the wino mass. The value of $\tan\beta$ comes from Yukawa coupling constant $f_{l_j} \sim 1/\cos\beta$ and v.e.v. of h_2, $v\sin\beta$.

Fig. 3

Feynman diagrams for the process $l_j \to l_i\gamma$. (a) represents the contributions from neutralino $\tilde{\chi}^0_A$ and slepton $\tilde{l}_X$ loop, and (b) the contributions from chargino $\tilde{\chi}^-_A$ and sneutrino $\tilde{\nu}_X$ loop.

Fig. 4

Penguin-type diagrams for the process $l_j^- \to l_i^- l_i^- l_i^+$ in which photon γ and Z-boson are exchanged. The blob indicates l_j-l_i-γ vertex such as Fig.3 or l_j-l_i-Z vertex where Z-boson is external.

Fig. 5

Box-type diagrams for the process $l_j^- \to l_i^- l_i^- l_i^+$. Here, (a) represents the contributions from neutralino $\tilde{\chi}_A^0$ and slepton $\tilde{l}_X$ loop, while (b) the contributions from chargino $\tilde{\chi}_A^-$ and sneutrino $\tilde{\nu}_X$ loop.

Fig. 6

Feynman diagrams for the process μ-e conversion at the quark level. In (a), the Penguin-type diagram is depicted. The blob indicates l_j-l_i-γ vertex such as Fig. 3 or l_j-l_i-Z vertex such as Fig. 4. In (b) and (c), the box-type diagrams are depicted; *i.e.*, (b) represents the contributions from neutralino $\tilde{\chi}_A^0$, slepton $\tilde{l}_X$ and squark $\tilde{q}_X$ $(q = u, d)$ loop, and (c) the contributions from chargino $\tilde{\chi}_A^-$, sneutrino $\tilde{\nu}_X$ and squark $\tilde{q}_X$ $(q = u, d)$ loop.

Fig. 7

The values of the SUSY contribution to the anomalous magnetic dipole-moment of muon $(g-2)_\mu^{SUSY}$ as a function of the left-handed selectron mass with the D-term contribution, which we denote by $m_{\tilde{e}_L}$. Here we assume $a = 0$ at the gravitational scale. Real lines correspond to the case for $\mu > 0$, while dashed lines for $\mu < 0$. Here we have taken $M_2 = 100$ GeV and $\tan\beta = 3,\ 10,\ 30$. The shaded regions are excluded by the present experiments.

Fig. 8

Branching ratios for the process $\mu \to e\gamma$ in the *Case 1*) $V = V_{KM}$ as a function of the left-handed selectron mass with the D-term contribution, $m_{\tilde{e}_L}$. Real lines correspond to the case for $\mu > 0$, while dashed lines for $\mu < 0$. Here we have taken $M_2 = 100$ GeV and $\tan\beta = 3,\ 10,\ 30$. We also show the present experimental upper bound for this process by the dash-dotted line.

Fig. 9

Same as Fig. 8 except for $M_2 = 200$ GeV.

Fig. 10

Branching ratios for the process $\mu^- \to e^- e^- e^+$ in the *Case 1)* $V = V_{KM}$ as a function of the left-handed selectron mass with the D-term contribution, $m_{\tilde{e}_L}$. Real lines correspond to the case for $\mu > 0$, while dashed lines for $\mu < 0$. Here we have taken $M_2 = 100$ GeV and $\tan\beta = 3,\ 10,\ 30$. We also show the present experimental upper bound for this process by the dash-dotted line.

Fig. 11

The μ-e conversion rates in nuclei $^{48}_{22}$Ti in the *Case 1)* $V = V_{KM}$ as a function of the left-handed selectron mass with the D-term contribution, $m_{\tilde{e}_L}$. Real lines correspond to the case for $\mu > 0$, while dashed lines for $\mu < 0$. Here we have taken $M_2 = 100$ GeV and $\tan\beta = 3,\ 10,\ 30$. We also show the present experimental upper bound for this process by the dash-dotted line.

Fig. 12

Branching ratios for the process $\tau \to \mu\gamma$ in the *Case 1)* $V = V_{KM}$ as a function of the left-handed selectron mass with the D-term contribution, $m_{\tilde{e}_L}$. Real lines correspond to the case for $\mu > 0$, while dashed lines for $\mu < 0$. Here we have taken $M_2 = 100$ GeV and $\tan\beta = 3,\ 10,\ 30$. We also show the present experimental upper bound for this process by the dash-dotted line.

Fig. 13

Branching ratios for the process $\tau \to \mu\gamma$ in the *Case 2)* neutrino mixing implied by atmospheric neutrino deficit, as a function of the left-handed selectron mass with the D-term contribution, $m_{\tilde{e}_L}$. Real lines correspond to the case for $\mu > 0$, while dashed lines for $\mu < 0$. Here we have taken $M_2 = 100$ GeV and $\tan\beta = 3,\ 10,\ 30$. We also show the present experimental upper bound for this process by the dash-dotted line.

Fig. 14

Branching ratios for the process $\mu \to e\gamma$ in the case for the minimal $SU(5)$ grand unified theory, as a function of the right-handed selectron mass with the D-term contribution, $m_{\tilde{e}_R}$. Here we have taken $\mu > 0$, $M_2 = 100$ GeV, and $\tan\beta = 3,\ 10,\ 30$. We also show

the present experimental upper bound for this process by the dash-dotted line.

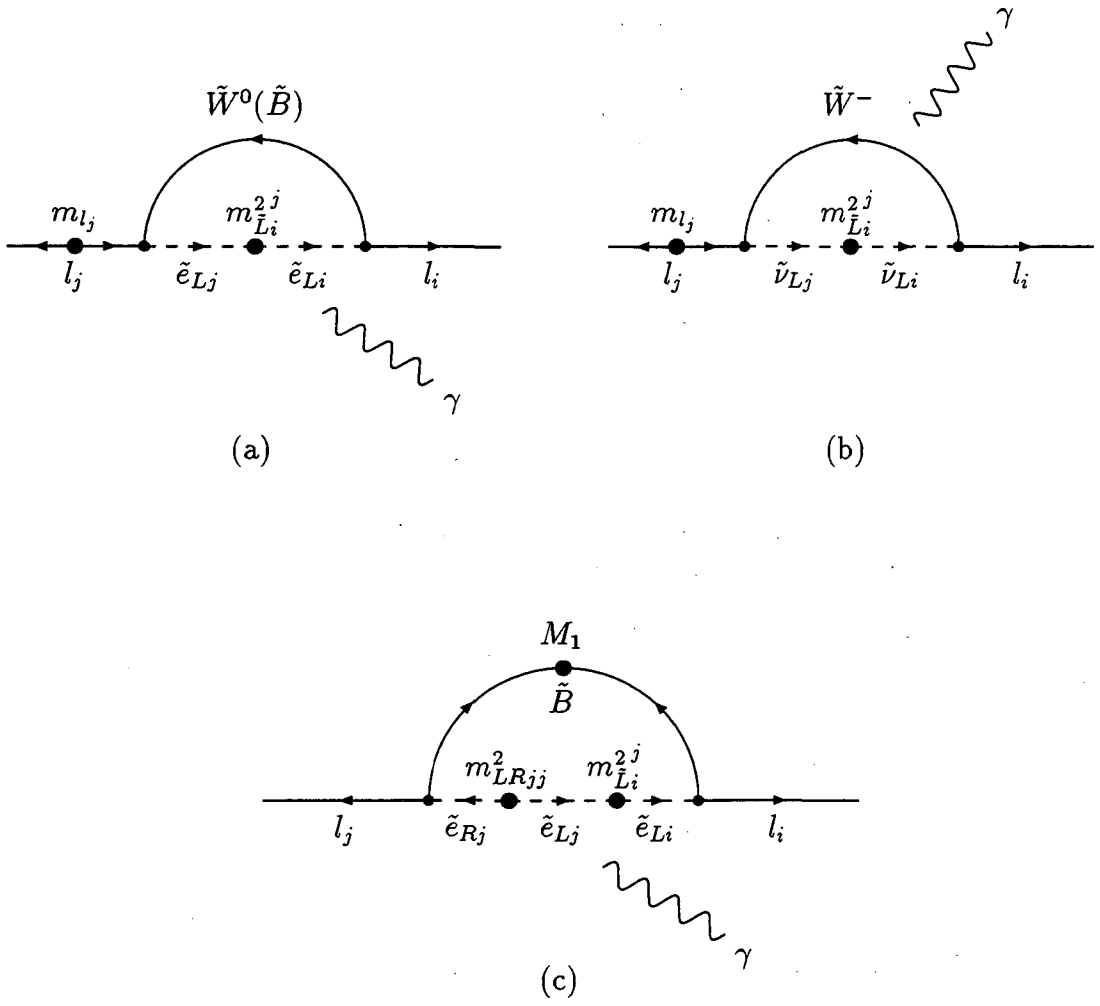
$\tilde{W}^0(\tilde{B})$
m_{l_j}
$m^{2\,j}_{\tilde{L}i}$
l_j
$\tilde{e}_{Lj}$
$\tilde{e}_{Li}$
l_i
γ
(a)
$\tilde{W}^-$
γ
m_{l_j}
$m^{2\,j}_{\tilde{L}i}$
l_j
$\tilde{\nu}_{Lj}$
$\tilde{\nu}_{Li}$
l_i
(b)
M_1
$\tilde{B}$
m^2_{LRjj}
$m^{2\,j}_{\tilde{L}i}$
l_j
$\tilde{e}_{Rj}$
$\tilde{e}_{Lj}$
$\tilde{e}_{Li}$
l_i
γ
(c)

Fig. 1

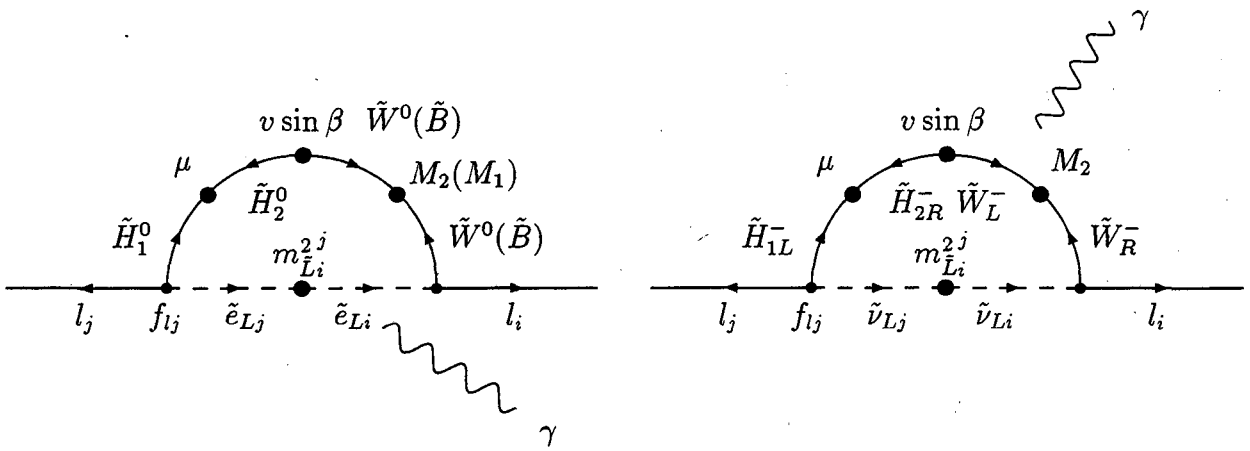
$v \sin\beta$
$\tilde{W}^0(\tilde{B})$
μ
$M_2(M_1)$
$\tilde{H}_2^0$
$\tilde{H}_1^0$
$m^{2\,j}_{\tilde{L}i}$
$\tilde{W}^0(\tilde{B})$
l_j
f_{lj}
$\tilde{e}_{Lj}$
$\tilde{e}_{Li}$
l_i
γ
γ
$v \sin\beta$
μ
M_2
$\tilde{H}_{2R}^-$
$\tilde{W}_L^-$
$\tilde{H}_{1L}^-$
$m^{2\,j}_{\tilde{L}i}$
$\tilde{W}_R^-$
l_j
f_{lj}
$\tilde{\nu}_{Lj}$
$\tilde{\nu}_{Li}$
l_i

(a) (b)

Fig. 2

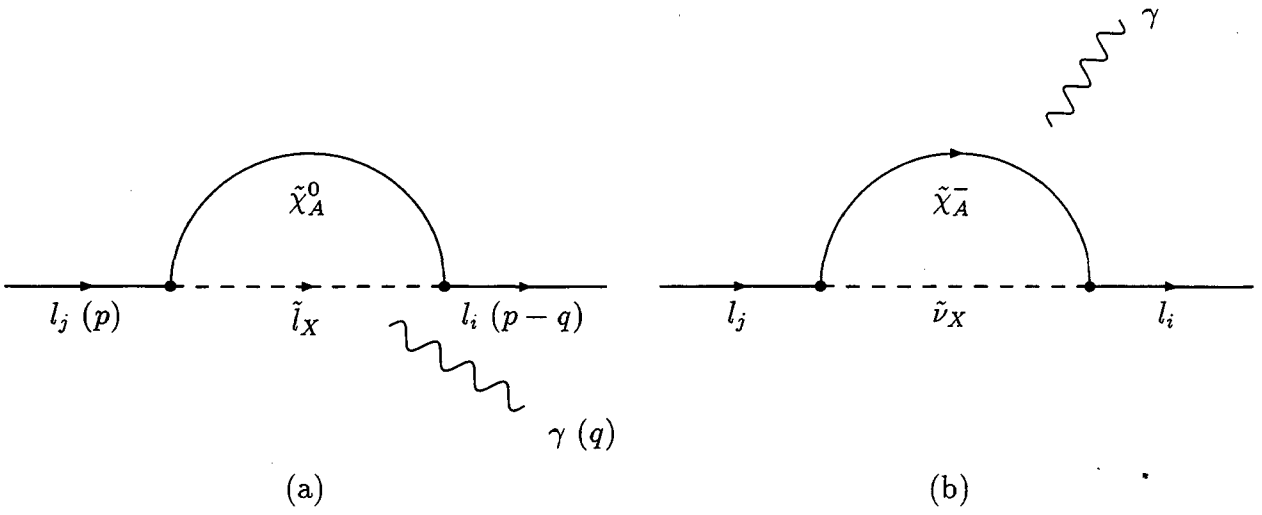
$\tilde{\chi}_A^0$
$l_j\ (p)$
$\tilde{l}_X$
$l_i\ (p-q)$
$\gamma\ (q)$
(a)
γ
$\tilde{\chi}_A^-$
l_j
$\tilde{\nu}_X$
l_i
(b)

Fig. 3

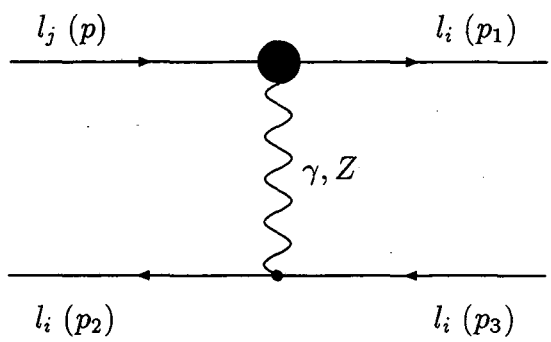

Fig. 4

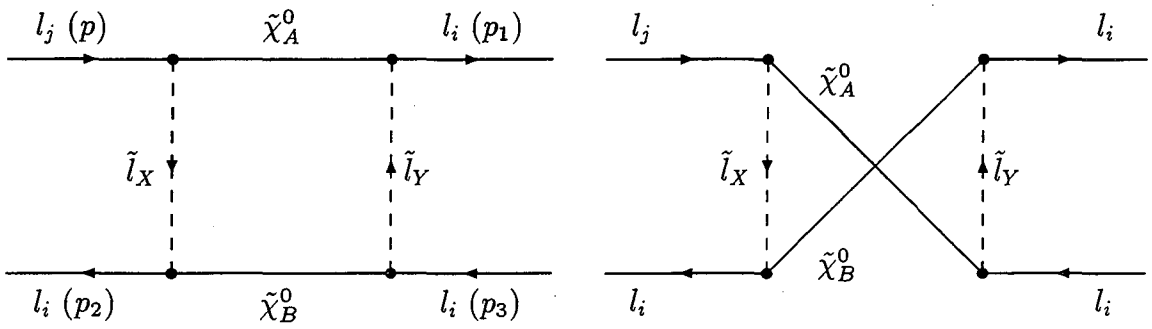
l_j (p)
$\tilde{\chi}^0_A$
l_i (p_1)
$\tilde{l}_X$
$\tilde{l}_Y$
l_i (p_2)
$\tilde{\chi}^0_B$
l_i (p_3)
l_j
l_i
$\tilde{\chi}^0_A$
$\tilde{l}_X$
$\tilde{l}_Y$
$\tilde{\chi}^0_B$
l_i
l_i

(a)

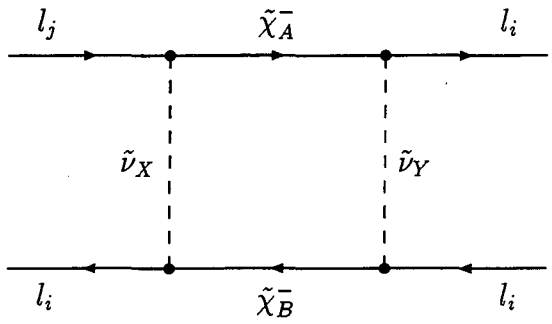
l_j
$\tilde{\chi}^-_A$
l_i
$\tilde{\nu}_X$
$\tilde{\nu}_Y$
l_i
$\tilde{\chi}^-_B$
l_i

(b)

Fig. 5

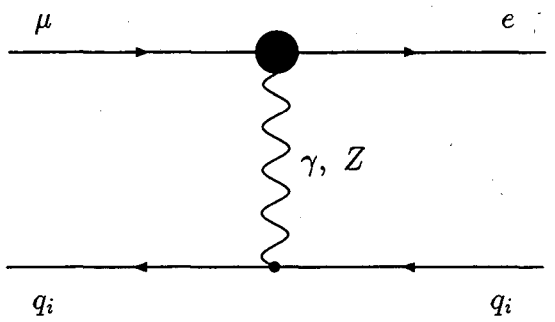
μ
e
$\gamma,\ Z$
q_i
q_i

(a)

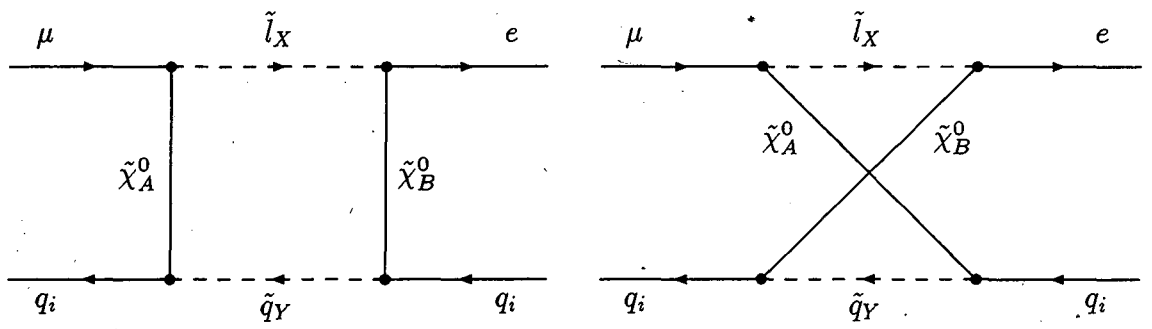
μ
$\tilde{l}_X$
e
$\tilde{\chi}^0_A$
$\tilde{\chi}^0_B$
q_i
$\tilde{q}_Y$
q_i
μ
$\tilde{l}_X$
e
$\tilde{\chi}^0_A$
$\tilde{\chi}^0_B$
q_i
$\tilde{q}_Y$
q_i

(b)

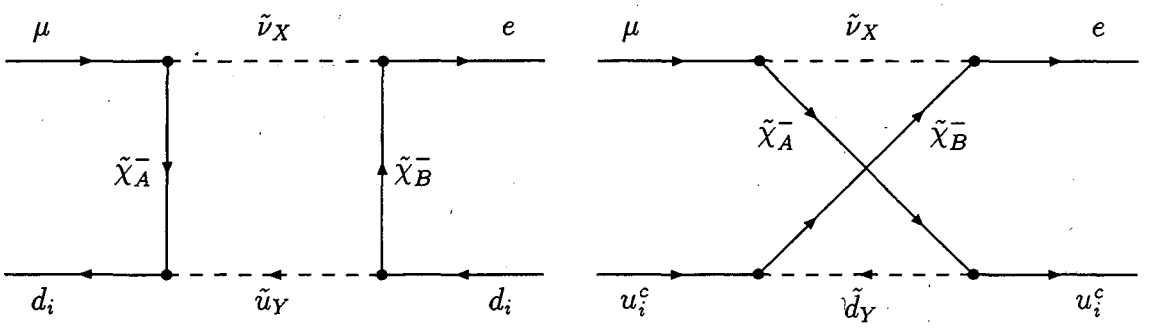
μ
$\tilde{\nu}_X$
e
$\tilde{\chi}^-_A$
$\tilde{\chi}^-_B$
d_i
$\tilde{u}_Y$
d_i
μ
$\tilde{\nu}_X$
e
$\tilde{\chi}^-_A$
$\tilde{\chi}^-_B$
u^c_i
$\tilde{d}_Y$
u^c_i

(c)

Fig. 6

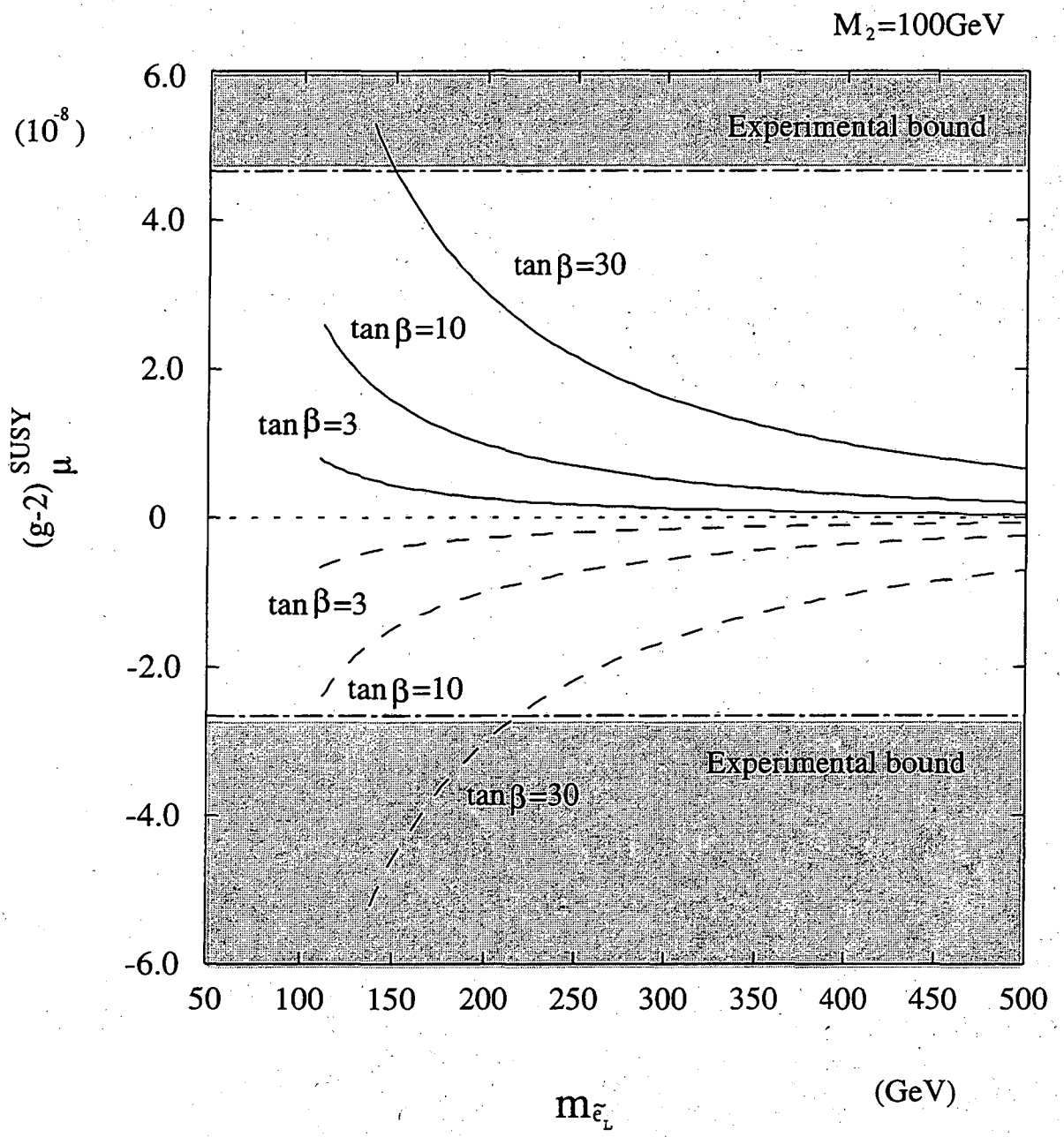
M2=100GeV
(10^-8)
6.0
4.0
2.0
0
-2.0
-4.0
-6.0
(g-2)μ SUSY
Experimental bound
tan β=30
tan β=10
tan β=3
tan β=3
tan β=10
tan β=30
Experimental bound
50
100
150
200
250
300
350
400
450
500
m ẽL
(GeV)

Fig. 7

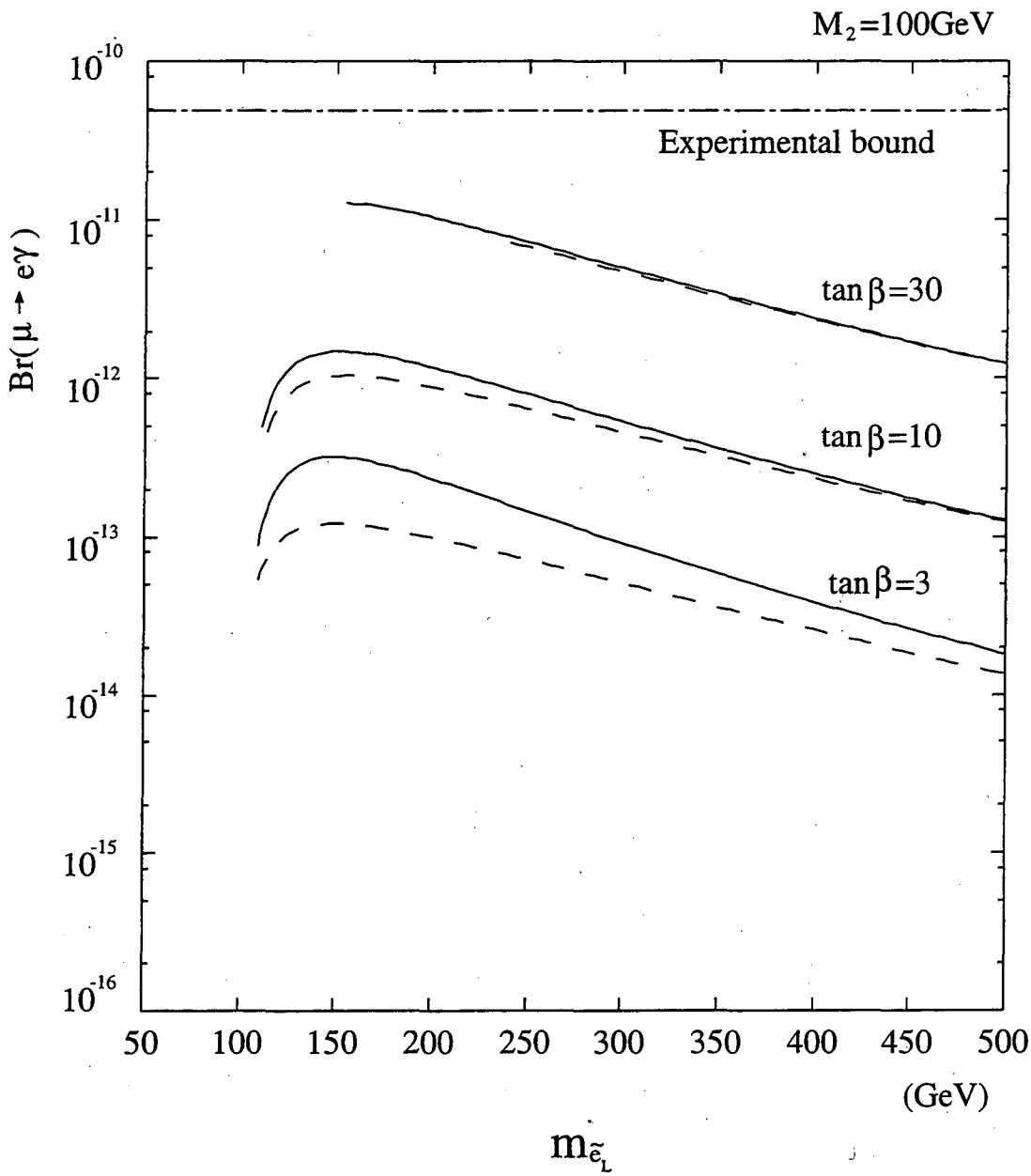
M2=100GeV
Experimental bound
tan β=30
tan β=10
tan β=3
Br(μ → eγ)
10^-10
10^-11
10^-12
10^-13
10^-14
10^-15
10^-16
50
100
150
200
250
300
350
400
450
500
(GeV)
m_ẽL

Fig. 8

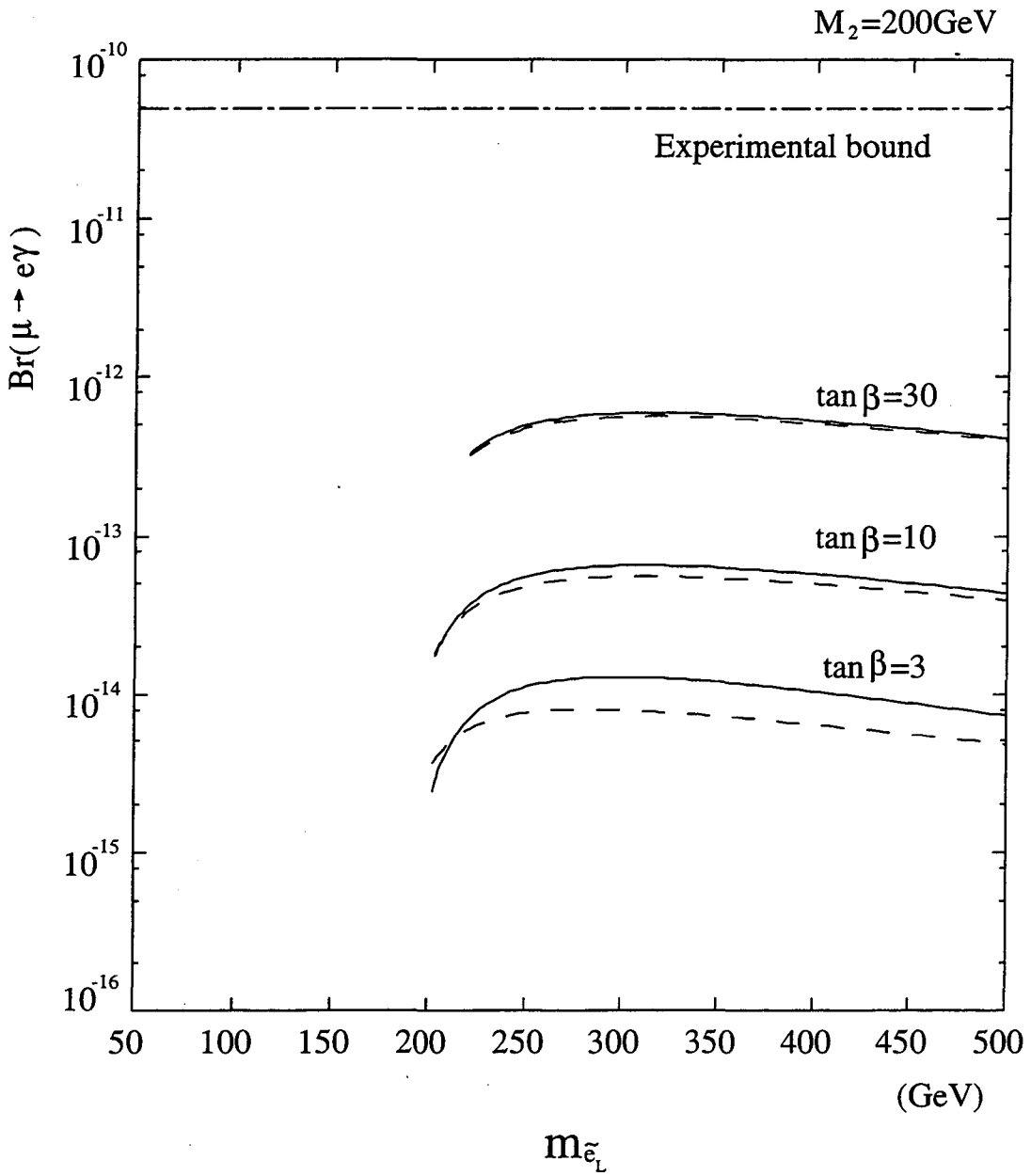
M2=200GeV
Experimental bound
tan β=30
tan β=10
tan β=3
Br(μ → eγ)
10-10
10-11
10-12
10-13
10-14
10-15
10-16
50
100
150
200
250
300
350
400
450
500
(GeV)
mẽL

Fig. 9

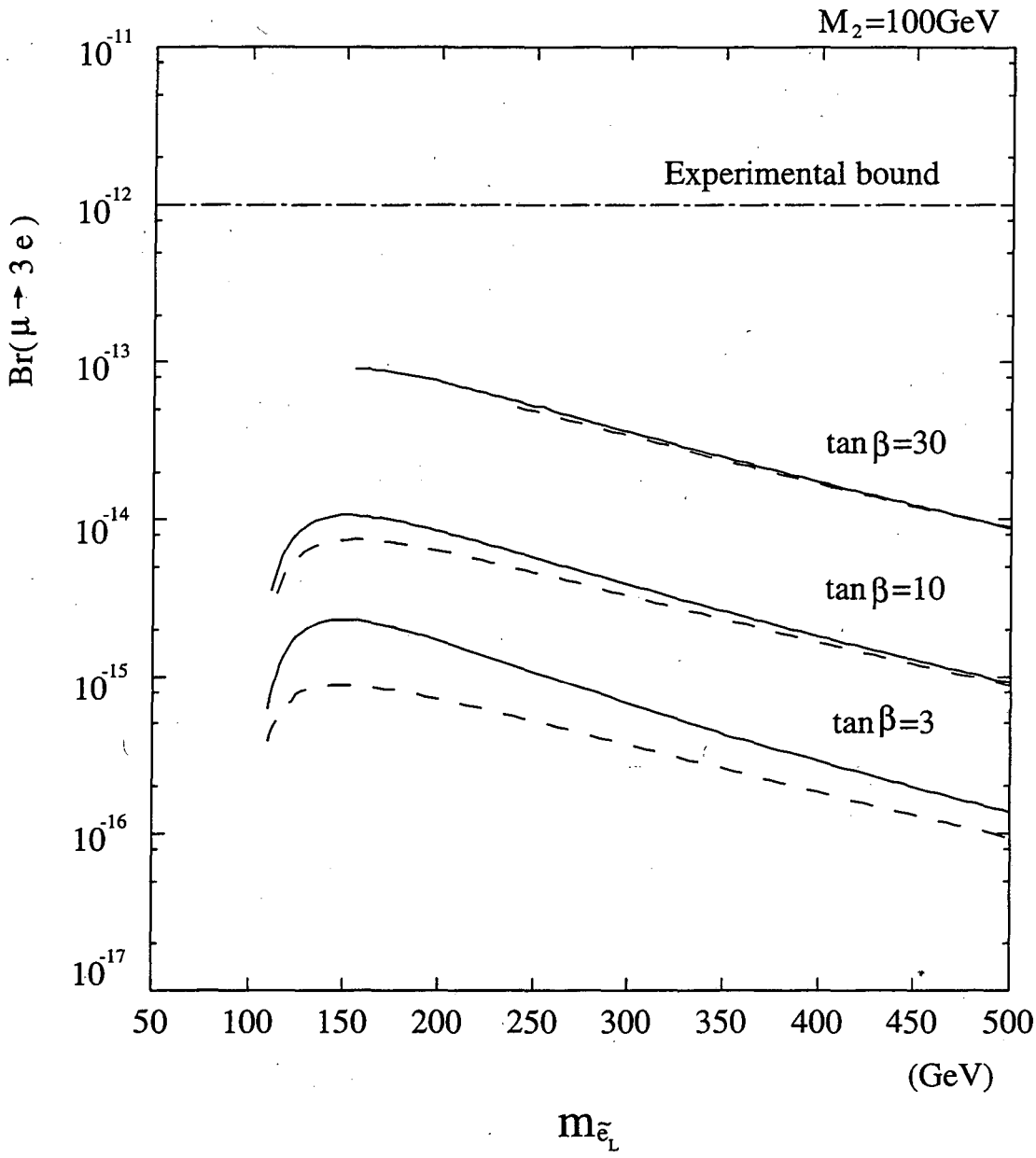
M2=100GeV
Experimental bound
Br(μ → 3 e)
10-11
10-12
10-13
10-14
10-15
10-16
10-17
tan β=30
tan β=10
tan β=3
50
100
150
200
250
300
350
400
450
500
(GeV)
mẽL

Fig. 10

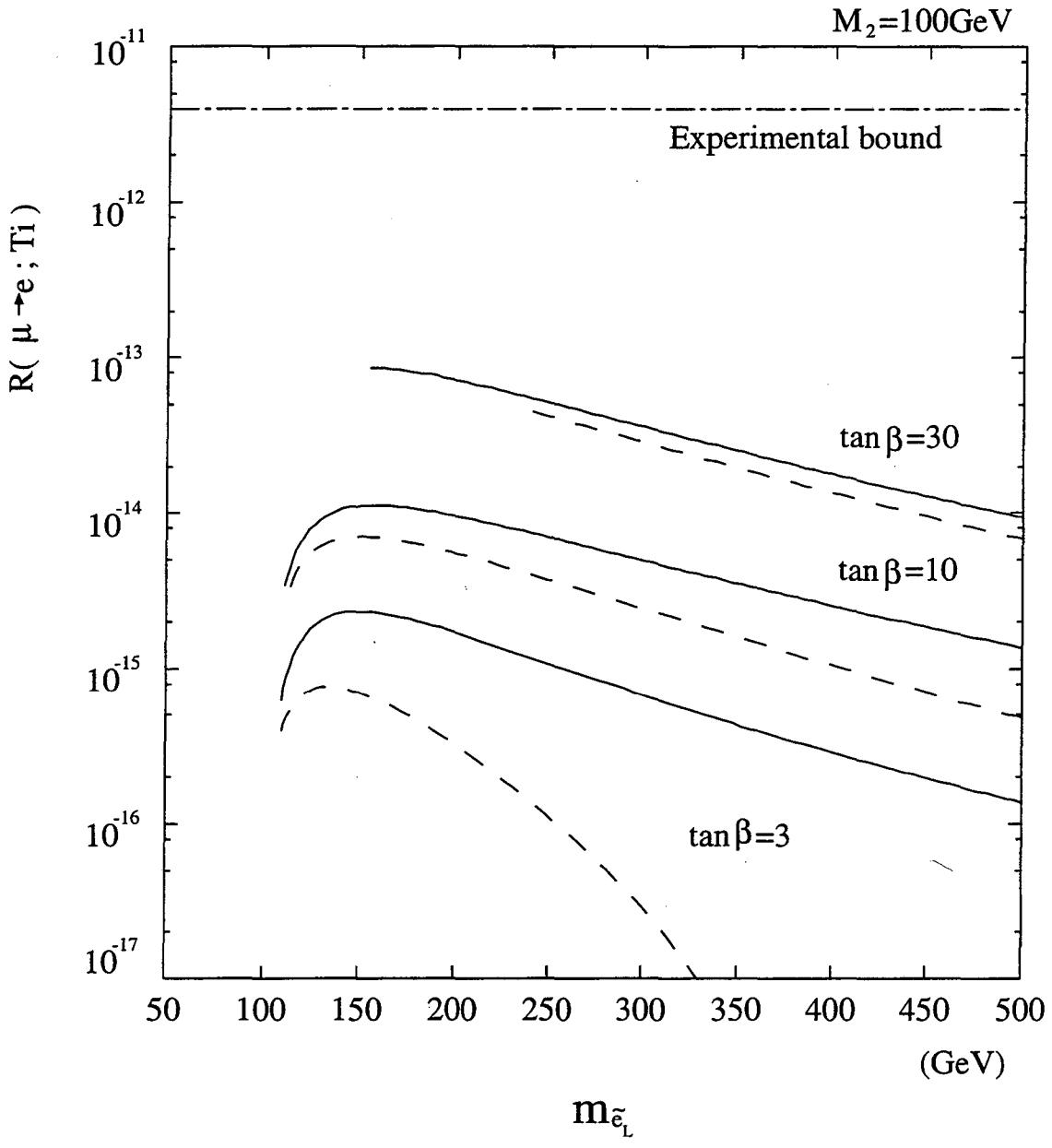
M2=100GeV
Experimental bound
R(μ→e ; Ti)
10-11
10-12
10-13
10-14
10-15
10-16
10-17
tan β=30
tan β=10
tan β=3
50
100
150
200
250
300
350
400
450
500
(GeV)
m ẽL

Fig. 11

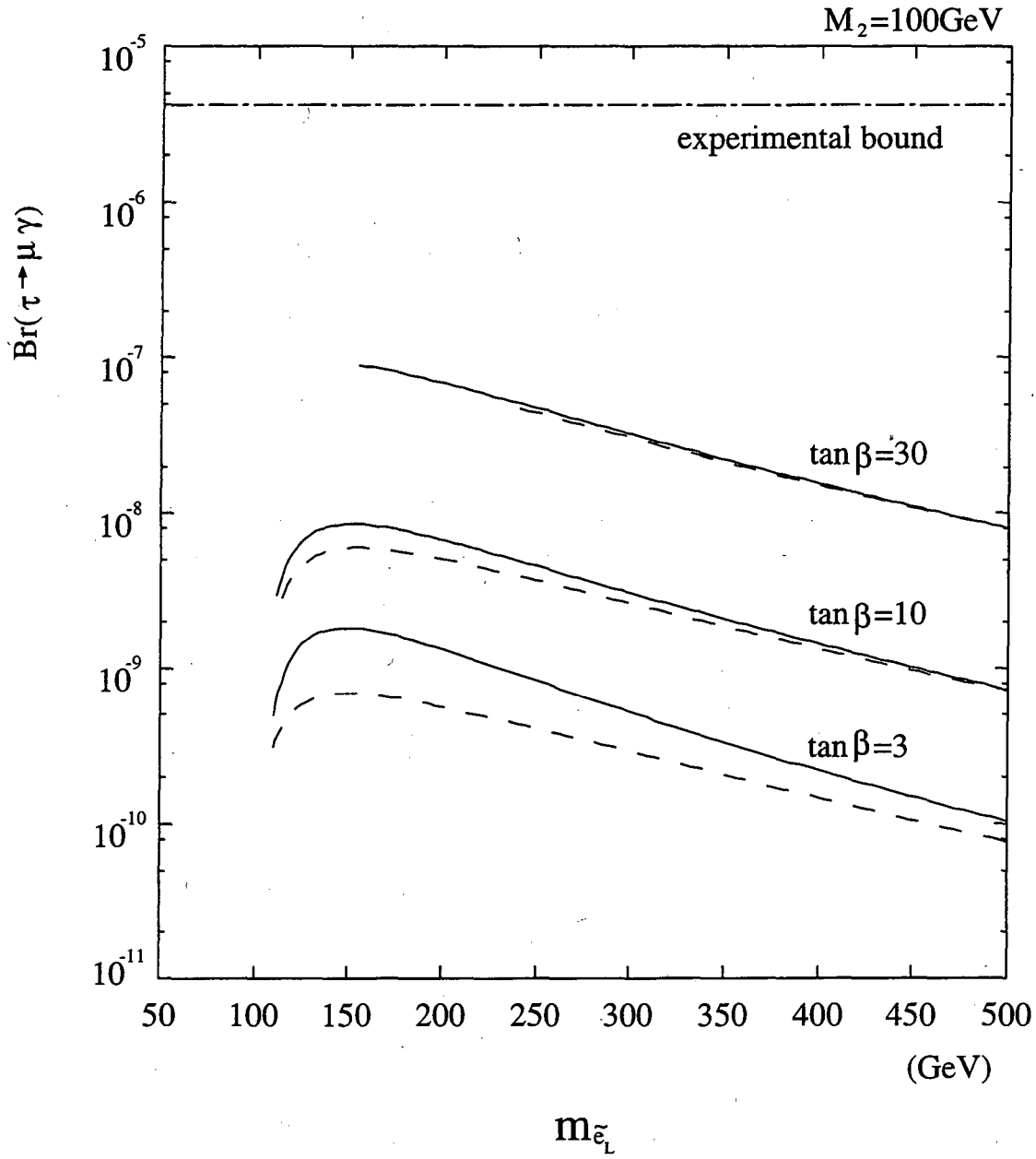
M2=100GeV
experimental bound
tan β=30
tan β=10
tan β=3
Br(τ→μγ)
10^-5
10^-6
10^-7
10^-8
10^-9
10^-10
10^-11
50
100
150
200
250
300
350
400
450
500
(GeV)
m_ẽL

Fig. 12

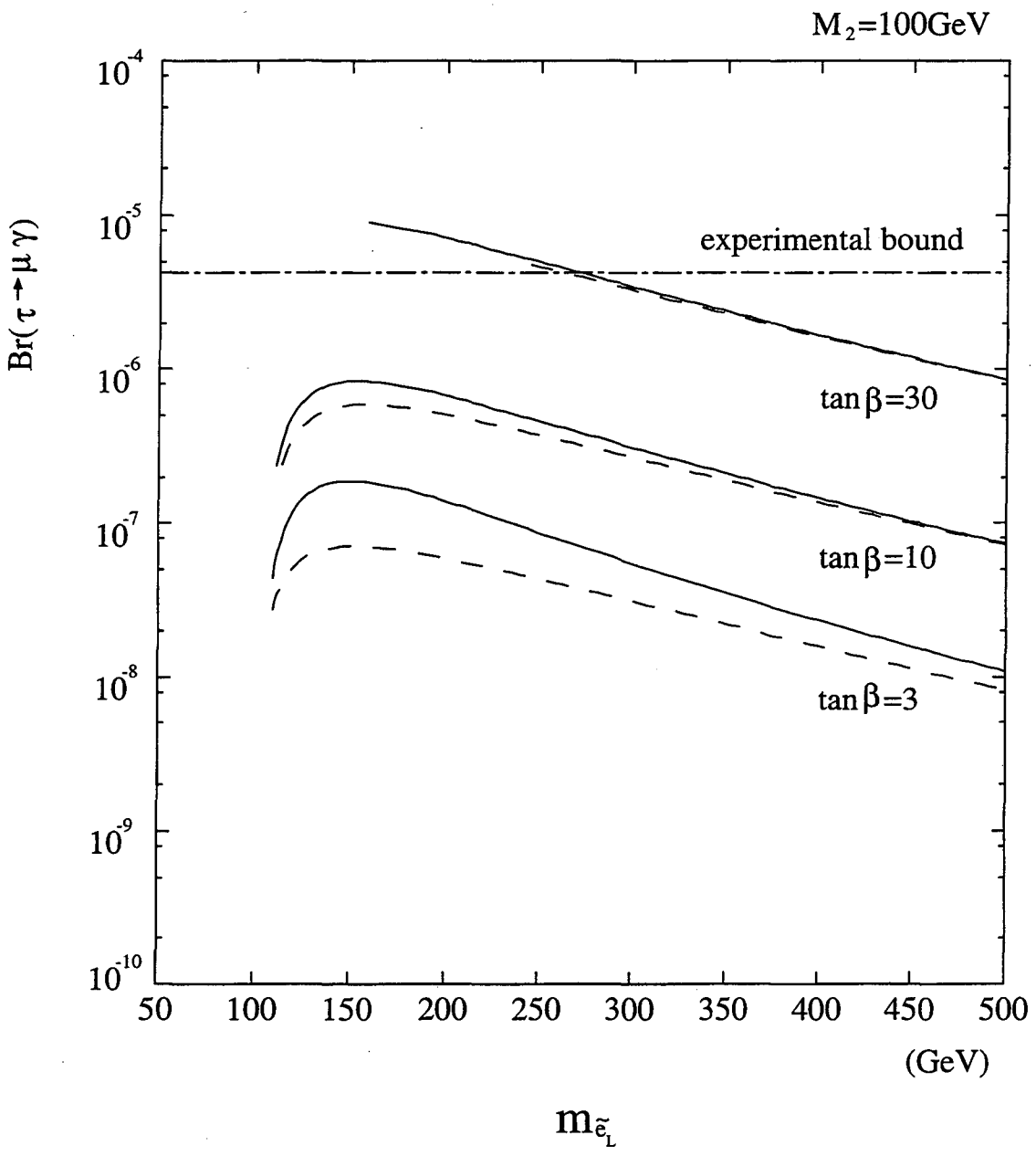
M2=100GeV
experimental bound
tan β=30
tan β=10
tan β=3
Br(τ→μγ)
10^-4
10^-5
10^-6
10^-7
10^-8
10^-9
10^-10
50
100
150
200
250
300
350
400
450
500
(GeV)
m_ẽL

Fig. 13

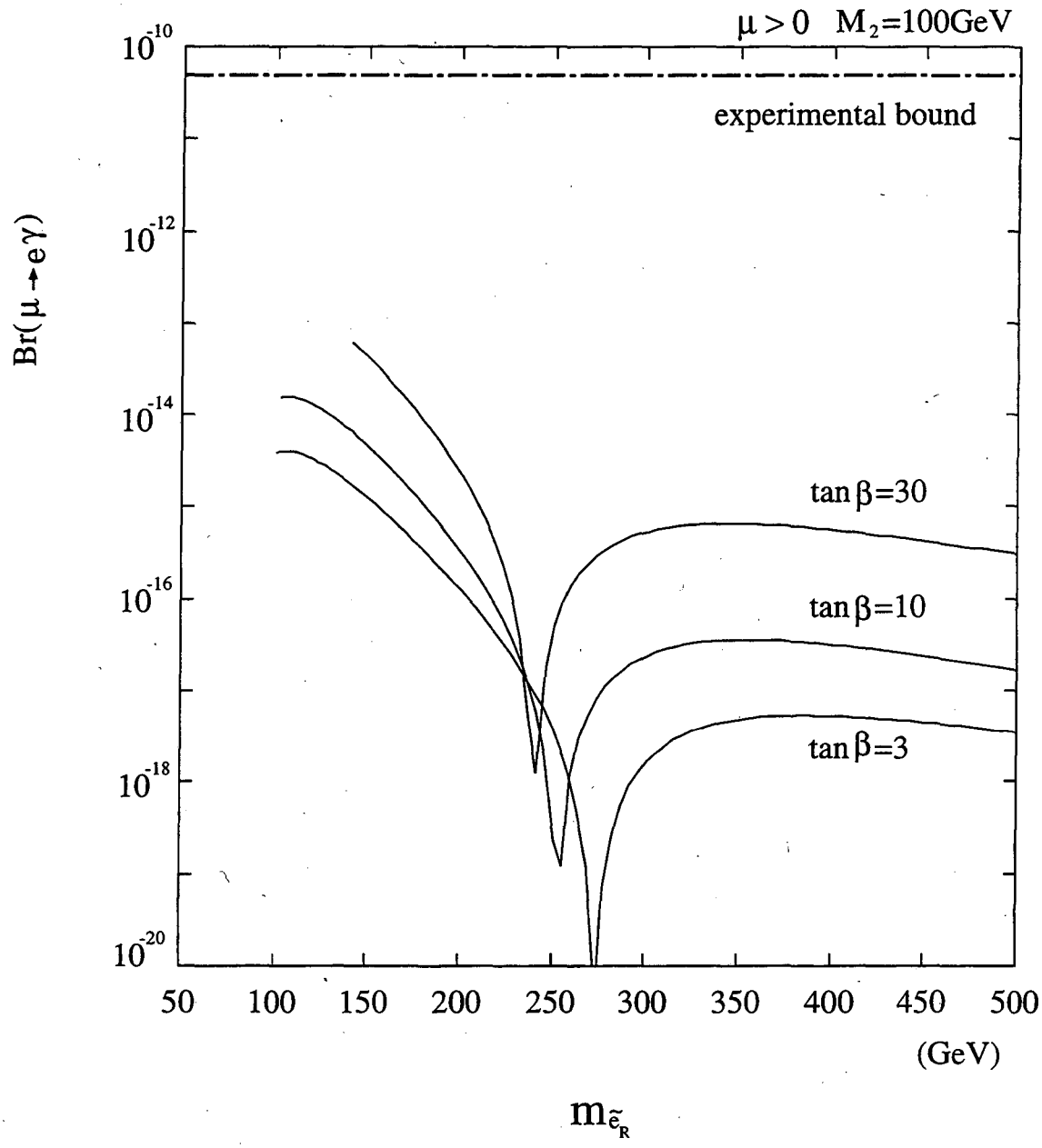
μ > 0 M2=100GeV
experimental bound
Br(μ→eγ)
10-10
10-12
10-14
10-16
10-18
10-20
tan β=30
tan β=10
tan β=3
50
100
150
200
250
300
350
400
450
500
(GeV)
mẽR

Fig. 14

LAWRENCE BERKELEY NATIONAL LABORATORY
UNIVERSITY OF CALIFORNIA
TECHNICAL & ELECTRONIC INFORMATION DEPARTMENT
BERKELEY, CALIFORNIA 94720